ELSEVIER

Physica D 134 (1999) 1–47

PHYSICA D

www.elsevier.com/locate/physd

Sources, sinks and wavenumber selection in coupled CGL equations and experimental implications for counter-propagating wave systems

Martin van Hecke [a,*], Cornelis Storm [b], Wim van Saarloos [b]

[a] *Center for Chaos and Turbulence Studies, The Niels Bohr Institute, Blegdamsvej 17, 2100 Copenhagenø, Denmark*
[b] *Instituut–Lorentz, Leiden University, P.O. Box 9506, 2300 RA Leiden, The Netherlands*

Received 4 June 1998; received in revised form 16 February 1999; accepted 23 March 1999
Communicated by A.C. Newell

Abstract

We study the coupled complex Ginzburg–Landau (CGL) equations for traveling wave systems, and show that sources and sinks are the important coherent structures that organize much of the dynamical properties of traveling wave systems. We focus on the regime in which sources and sinks separate patches of left and right-traveling waves, i.e., the case that these modes suppress each other. We present in detail the framework to analyze these coherent structures, and show that the theory predicts a number of general properties which can be tested directly in experiments. Our counting arguments for the multiplicities of these structures show that independently of the precise values of the coefficients in the equations, there generally exists a symmetric stationary source solution, which sends out waves with a unique frequency and wave number. Sinks, on the other hand, occur in two-parameter families, and play an essentially passive role, being sandwiched between the sources. These simple but general results imply that sources are important in organizing the dynamics of the coupled CGL equations. Simulations show that the consequences of the wavenumber selection by the sources is reminiscent of a similar selection by spirals in the 2D complex Ginzburg–Landau equations; sources can send out stable waves, convectively unstable waves, or absolutely unstable waves. We show that there exists an additional dynamical regime where both single- and bimodal states are unstable; the ensuing chaotic states have no counterpart in single amplitude equations. A third dynamical mechanism is associated with the fact that the width of the sources does not show simple scaling with the growth rate ε. This is related to the fact that the standard coupled CGL equations are *not* uniform in ε. In particular, when the group velocity term dominates over the linear growth term, no stationary source can exist; however, sources displaying nontrivial dynamics can often survive here. Our results for the existence, multiplicity, wavelength selection, dynamics and scaling of sources and sinks and the patterns they generate are easily accessible by experiments. We therefore advocate a study of the sources and sinks as a means to probe traveling wave systems and compare theory and experiment. In addition, they bring up a large number of new research issues and open problems, which are listed explicitly in the concluding section.

PACS: 47.54.+r; 03.40.Kf; 47.20.Bp; 47.20.Ky

Keywords: Pattern formation; Coherent structures; Traveling waves; Sources

* Corresponding author.
E-mail address: mvhecke@nbi.dk (M.v. Hecke)

0167-2789/99/$ – see front matter
PII: S0167-2789(99)00068-8

1. Introduction

Many spatially extended systems display the formation of patterns when driven sufficiently far from equilibrium [1–5]. Examples include convection [2], interfacial growth phenomena [6,7] like directional solidification [8] and eutectic growth [9], chemical Turing patterns [2,5,10], the printer instability [11–13], patterns in liquid crystals [14], and even biophysical systems [15]. In the typical setup, the homogeneous equilibrium state turns unstable when a control parameter R (such as the temperature difference between top and bottom in Rayleigh–Bénard convection) is increased beyond a critical value R_c. If the amplitude of the patterns grows continuously when R is increased beyond R_c, the bifurcation is called supercritical (forward), and a weakly nonlinear analysis can be performed around the bifurcation point. A systematic expansion in the small dimensionless control parameter $\varepsilon := (R - R_c)/R_c$ yields amplitude equations that describe the slow, large-scale deformations of the basic patterns.

Because near threshold the form of the amplitude or envelope equation depends mainly on the symmetries and on the nature of the primary bifurcation (stationary or Hopf, finite wavelength or not, etc.), the amplitude description has become an important organizing principle of the theory of non-equilibrium pattern formation. Many qualitative and quantitative predictions have been successfully confronted with experiments [2–5]. Even outside their range of strict applicability, i.e., for finite values of ε, the amplitude equations are often the simplest nontrivial models satisfying the symmetries of the underlying physical system. As such, they can be studied as general models of nonequilibrium pattern formation.

The most detailed comparison between the predictions of an amplitude description and experiments has been made [2] for the type of systems for which the theory was originally developed [1], hydrodynamic systems that bifurcate to a stationary periodic pattern (critical wavenumber $q_c \neq 0$ and critical frequency $\omega_c = 0$). The corresponding amplitude equation has real coefficients and takes the form of a Ginzburg–Landau equation; it is often referred to as the real Ginzburg–Landau equation. The coefficients occurring in this equation set length and time scales only, and for a theoretical analysis of an infinite system, they can be scaled away. Hence one equation describes a variety of experimental situations and the theoretical predictions have been compared in detail with the experimental observations in a number of cases [2–5].

For traveling wave systems (critical wavenumber $q_c \neq 0$ and critical frequency $\omega_c \neq 0$), there are, however, few examples of a direct confrontation between theory and experiment, since the qualitative dynamical behavior depends *strongly* on the various coefficients that enter the resulting amplitude equations [1]. The calculations of these coefficients from the underlying equations of motion are rather involved and have only been carried out for a limited number of systems [21–25], and in many experimental cases the values of these coefficients are not known. A different problem generally arises when dealing with systems of counter-propagating waves, where in many cases the standard coupled amplitude equations (2) and (3) are not uniformly valid in ε. Therefore one has to be cautious about the interpretation of results based on these equations [26–32]. We return to this issue in Section 1.2.2.

It is the main goal of this paper to show that the theory, based on the standard coupled amplitude equations (2) and (3), *does* predict a number of generic properties of sources and sinks which can be directly tested experimentally. In fact, as the results of [33] for traveling waves near a heated wire also show, *sources* and *sink* type solutions are the ideal coherent structures to probe the applicability of the coupled amplitude equations to experimental systems. The reason is that these coherent structures are, by their very nature, based on a competition between left and right-traveling waves in the bulk, and, unlike wall or end effects, they do not depend sensitively on the experimental details. Moreover, a study of their scaling properties not only yields experimentally testable predictions, but also bears on the relation between the averaged amplitude equations and the standard amplitude equations (see Sections 1.2.2 and 4). Finally, as we shall discuss, one of our main points is consistent with something which is visible in

[1] In practice complications may also arise due to the presence of additional important slow variables [16–20].

many experiments, namely that the sources determine the wavelength in the patches between sources and sinks, and hence organize much of the dynamics.

Sources and sinks have been observed in a wide variety of experimental systems where oppositely traveling waves suppress each other, especially in convection [26,33–42]. An example of a one-dimensional source in a chemical system is given in [43]. To our knowledge, however, they have *not* been explored systematically in most of these systems. In fact, many experimentalists who study traveling wave systems focus on the single-mode case – by perturbing the system or quenching the control parameter ε it is in general possible to eliminate the sources and sinks.

Theoretically, some properties of sources and sinks in coupled amplitude equations have been analyzed by many workers [26–33,44–55]. We shall briefly review some of these results in Section 1.2. To our knowledge, however, there have been very little systematic studies comparing theory and experiment, and we therefore advocate a study of these coherent structures as a means to probe traveling wave systems. The two main objectives of this paper are to expand the detailed analysis and reasoning underlying the arguments of [33], and to stimulate experimental investigations along such lines for other systems as well.

1.1. The coupled complex Ginzburg–Landau equations

When both the critical wavenumber q_c and the critical frequency ω_c are nonzero at the pattern forming bifurcation, the primary modes are traveling waves and the generic amplitude equations are complex Ginzburg–Landau (CGL) equations. When these primary modes are essentially one-dimensional and the system possesses left–right reflection symmetry, the weakly nonlinear patterns are of the form

$$\text{physical fields} \propto A_R e^{-i(\omega_c t - q_c x)} + A_L e^{-i(\omega_c t + q_c x)} + \text{c.c.}, \tag{1}$$

where A_R and A_L are the complex-valued amplitudes of the right and left-traveling waves. Following arguments from general bifurcation theory, i.e., anticipating that these amplitudes are of order $\varepsilon^{1/2}$ and that they vary on slow temporal and spatial scales, one then finds that the appropriate amplitude equations for traveling wave systems with left–right symmetry are the coupled CGL equations [2,5,26–29,56]

$$\partial_t A_R + s_0 \partial_x A_R = \varepsilon A_R + (1 + ic_1)\partial_x^2 A_R - (1 - ic_3)|A_R|^2 A_R - g_2(1 - ic_2)|A_L|^2 A_R, \tag{2}$$

$$\partial_t A_L - s_0 \partial_x A_L = \varepsilon A_L + (1 + ic_1)\partial_x^2 A_L - (1 - ic_3)|A_L|^2 A_L - g_2(1 - ic_2)|A_R|^2 A_L. \tag{3}$$

In these equations, we have used the freedom to choose appropriate units of length, time and of the amplitudes to set various prefactors to unity. Our conventions are those of [2], except that we have, following [26], denoted the coupling coefficient of the two modes by g_2. Apart from the "control parameter" ε, there are five important coefficients occurring in these equations: c_1 and c_3 determine the linear and nonlinear dispersion of a single mode, c_2 determines the dispersive effect of one mode on the other, g_2 expresses the mutual suppression of the modes and s_0 is the *linear* group velocity of the traveling wave modes [2]. As a function of all these different coefficients, many different types of dynamics are found [2,57–59].

It is important to stress, following [26–32], that one has to be cautious about the range of validity of the coupled amplitude equations ((2) and (3)). When the linear group velocity s_0 is of order $\sqrt{\varepsilon}$, as happens near a co-dimension two point in binary mixtures [26] or lasers [60,61], then ε can be removed from the equations by an appropriate rescaling of space and time and the amplitude equations are valid uniformly in ε. However, in most realistic traveling

[2] It should be noted that by a rescaling one can either fix ε or s_0. Since ε can be varied experimentally, we usually keep s_0 at a fixed value and vary ε.

wave systems s_0 is of order unity, the amplitude equations do not scale uniformly with ε [26], and their validity is not guaranteed. In practice, the attitude towards this issue has often been (either implicitly or explicitly [62]) that as they respect the proper symmetries, the equations may well yield good descriptions of physical systems outside their proper range of validity.

Note in this regard that in a single patch of a left or right traveling wave a single amplitude equation for A_R or A_L suffices; in this case, the linear group velocity term $s_0\partial_x A_R$ or $s_0\partial_x A_L$ can be removed by a Galilean transformation. The issue of validity of the amplitude equations does not arise then (see the discussion in Section 5.3.2), and many theoretical studies have focused on this single CGL equation [63–65].

1.2. Historical perspective

In this section we will give a brief overview of earlier theoretical work on sources, sinks and coupled amplitude equations in as far as these pertain to our work. It should be noted that grain boundaries for 2D traveling waves, under the assumption of lateral translational symmetry, can be described as 1D sources and sinks [49,51]; hence some results relevant to the work here can be found in papers focusing on the 2D case. This explains the frequent references to early work on grain boundaries in 2D standing wave patterns [55]. Earlier experimental work will be discussed in the section on experimental relevance.

1.2.1. Earlier work on sources and sinks

Early examples of sources and sinks in the literature can be found in the work by Joets and Ribotta (see [44–46] and references therein), who studied these structures both in experiments on electroconvection in a nematic liquid crystal, and in simulations of coupled Ginzburg–Landau equations. They focus mainly on nucleation of sources and sinks, and multiplication processes. Sources and sinks have also been observed and studied in traveling waves in binary mixtures [37–39,41,42]. In this system, however, the transition is weakly subcritical. We will compare some of the results of these experiments with some of our findings in Section 6.2.2.

Theoretically, some properties of sources and sinks in coupled amplitude equations have also been analyzed by Cross [26,27], Coullet et al. [47,48], Malomed [49,50], Aranson and Tsimring [51] and others [33,52,53].

Coullet et al. [47] consider sources and sinks occurring in one- and two-dimensional coupled CGL equations from both a topological and numerical point of view. In particular, they observe numerically that patterns in which sources and sinks are present typically select a unique wavenumber, a feature which plays a central role in our discussion.

A particular important prediction of Coullet et al. [48] was that sources typically exist only a finite distance above threshold, for $\varepsilon > \varepsilon_c^{so} > 0$. The authors remark that below this threshold, the sources become very sensitive to noise, and an addition of noise to the coupled CGL equations was found to inhibit the divergence of sources in this case. Moreover, they predict that the width of sinks diverges as $1/\varepsilon$ in contrast to what was asserted in [26,27] or what was found perturbatively in the limit $s_0 \to 0$, ε finite [49]. There appears to have been neither a systematic numerical check of these predictions nor a comparison with experiments. In this paper we shall recover the existence of a critical value ε_c^{so} from a slightly different angle, and show that ε_c^{so} is only the critical value above which *stationary* source solutions exist. Below ε_c^{so} source-type structures *can* exist, but they are intrinsically dynamical and very large. We will refer to these structures as *non-stationary* sources, as opposed to the stationary ones we encounter above ε_c^{so}. As we will discuss in Section 1.2.2, the prediction of a *finite* critical value ε_c^{so} for sources from the lowest order amplitude equations is a priori questionable, but we shall argue that the existence of such a critical value is quite robust for systems where the bifurcation to traveling waves is supercritical. For systems where the bifurcation is subcritical, there need not be such a critical value ε_c^{so}. This may be the reason that in experiments on traveling waves in binary fluid convection [37], there does not appear to be evidence for the nonexistence of stationary sources below a nonzero value of ε_c^{so}.

Malomed [49] studied sources and sinks near the Real Ginzburg–Landau limit of the coupled CGL equations, and also found wavenumber selection. Aranson and Tsimring [51] considered domain walls occurring in a 2D version of the complex Swift–Hohenberg model. Assuming a translational invariance along this domain wall, one obtains as amplitude equations the coupled 1D CGL equations ((2) and (3)) with $s_0 = 1, c_1 \to \infty, c_2 = c_3 = 0$ and $g_2 = 2$. For that case, a unique source was found as well as a continuum of sinks. For the full 2D problem, a transverse instability typically renders these solutions unstable. Finally, Rovinsky et al. [52] studied the effects of boundaries and pinning on sinks and sources occurring in coupled CGL equations, and finally we note that some examples of sources in periodically forced systems are discussed by Lega and Vince [54].

1.2.2. Validity of the coupled CGL equations

There is quite some discussion about under what conditions the standard coupled amplitude equations (2) and (3) are valid for counter-propagating wave systems [28–32]. The essential observation is that when s_0 is finite, ε cannot be scaled out from the coupled amplitude equations (2) and (3).

Knobloch and De Luca [28,29] and Vega and Martel [30–32] found that under some conditions the amplitude equations for finite s_0 reduce to

$$\partial_t A_\mathrm{R} + s_0 \partial_x A_\mathrm{R} = \varepsilon A_\mathrm{R} + (1 + \mathrm{i}c_1)\partial_x^2 A_\mathrm{R} - (1 - \mathrm{i}c_3)|A_\mathrm{R}|^2 A_\mathrm{R} - g_2(1 - \mathrm{i}c_2)\langle |A_\mathrm{L}|^2 \rangle A_\mathrm{R}, \tag{4}$$

$$\partial_t A_\mathrm{L} - s_0 \partial_x A_\mathrm{L} = \varepsilon A_\mathrm{L} + (1 + \mathrm{i}c_1)\partial_x^2 A_\mathrm{L} - (1 - \mathrm{i}c_3)|A_\mathrm{L}|^2 A_\mathrm{L} - g_2(1 - \mathrm{i}c_2)\langle |A_\mathrm{R}|^2 \rangle A_\mathrm{L}. \tag{5}$$

in the limit $\varepsilon \to 0$, where $\langle |A_\mathrm{L}|^2 \rangle$ and $\langle |A_\mathrm{R}|^2 \rangle$ denote averages in the co-moving frames of the amplitudes A_R and A_L. Intuitively, the occurrence of the averages stems from the fact that the group velocity s_0 becomes infinite after scaling ε out of the equations; in other words, when we follow one mode in the frame moving with the group velocity, the other mode is swept by so quickly, that only its average value affects the slow dynamics. These equations have been used in particular to study the effect of boundary conditions and finite size effects [28–32], but for the study of sources and sinks they appear less appropriate since they are effectively decoupled single-mode equations with a renormalized linear growth term. Nevertheless, we shall see in Section 4 that in the small ε limit sources and sinks often disappear from the dynamics, and if so, these equations may yield an appropriate description of the late-stage regime.

1.2.3. Complex dynamics in coupled amplitude equations

In Section 5 we will discuss chaotic behavior that results from the source-induced wavenumber selection. Complex and chaotic behavior in the coupled amplitude equations has, to the best of our knowledge, received very little attention; notable exceptions are the papers by Sakaguchi [57,58], Amengual et al. [59] and van Hecke and Malomed [66].

In the papers of Sakaguchi [57,58], the coupled CGL equations ((2) and (3)) were studied in the regime where the cross-coupling coefficient g_2 is close to 1. It was pointed out that the transition between single and bimodal states in general shifts away from $g_2 = 1$ when the nonlinear waves show phase or defect chaos; in some cases this transition can become hysteretic. Furthermore, periodic states and tightly bound sink/source pairs that we will encounter in Section 5.2 were already obtained here.

In the recent work by Amengual et al. [59], two coupled CGL equations with group velocity s_0 equal to zero were studied. The dispersion coefficients c_1 and c_3 were chosen such that the uncoupled equations are in the spatio-temporal intermittent regime [63–65,67]. Upon increasing the coupling coefficient g_2, sink/source patterns were observed for $g_2 > 1$; in these patterns, no intermittency was observed. We will comment on this work in Section 5.3.2, and in particular give a simple explanation of the disappearance of the intermittency.

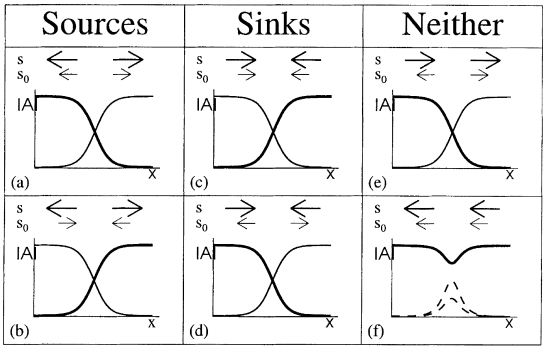

Fig. 1. Schematic representations of the various coherent structures that we will encounter in this paper. The amplitude of the left (right) traveling waves is indicated by a thick (thin) curve, while the linear group velocity and total group velocity are denoted by s_0 and s respectively, and their direction is indicated by arrows. (a) and (b) are, in our definition, both sources, since the nonlinear group velocity s points outward; the majority of cases that we will encounter will be of type (a). Similarly, (c) and (d) both represent sinks. Finally, one may in principal encounter structures that are neither sources nor sinks. We never have observed a structure of the form shown in (e) in our simulations, but structures like shown in (f) occur quite generally in the chaotic regimes. The dotted curve for the A_R mode indicates that we can have many different possibilities here, including the case were $A_R = 0$; in that case a description in terms of a single CGL equation suffices. Note that figure (f) does not exhaust all possibilities which are essentially single-mode structures. E.g., in our simulations presented in Fig. 3, we encounter a case where in between a source of type (a) and one of type (b) there is a single-mode sink, for which s points inwards.

1.3. Outline

After discussing the definition of sources and sinks of related coherent structures in Section 2 (p. 6), we turn to the counting analysis in Section 3 (p. 8). We focus in our presentation on the ingredients of the analysis and on the main results, relegating all technical details of the analysis to Appendices A and B (p. 36 and p. 40, respectively). The essential result is that one typically finds a unique symmetric source solution with zero velocity.

We discuss the scaling of the width of sources and sinks with ε in Section 4 (p. 12). The main result is that beyond the critical value ε_c^{so} sources are intrinsically non-stationary.

In Section 5 (p. 19), we discuss the stability of the waves sent out by the source solutions, and identify three different mechanisms that may lead to chaotic behavior. Furthermore we explore numerically some of the richness found in the coupled amplitude equations. We find a plethora of structures and possible dynamical regimes.

Finally, in Section 6 (p. 29), we close our paper by putting some of our results in perspective, also in relation to the experiments, and by discussing some open problems.

2. Definition of sources and sinks

Sources and sinks arise when the coupling coefficient g_2 is sufficiently large that one mode suppresses the other. Then the system tends to form domains of either left-moving or right-moving waves, separated by domain walls or shocks. The distinction between *sources* or *sinks* according to whether the nonlinear group velocity points s of the asymptotic plane waves points *outwards* or *inwards* (see Fig. 1) is crucial here. From a physical point of view, the group velocity determines the propagation of small perturbations. In our definition, a source is an "active" coherent structure which sends out waves to both sides, while a sink is sandwiched between traveling wave states with the group velocity pointing inwards; perturbations travel away from sources and into sinks. Mathematically, it will turn out that the distinction between sources and sinks in terms of the group velocity s is also precisely the one that is natural in the context of the counting arguments.

In an actual experiment concerning traveling waves, when one measures an order parameter and produces space–time plots of its time evolution, lines of constant intensity indicate lines of constant phase of the traveling waves (see for example [33,37–39]). The direction of the *phase velocity* $v_{\rm ph}$ of the waves in each single-mode domain is then immediately clear. Since s and $v_{\rm ph}$ do not have to have the same sign, one cannot distinguish sources and sinks based on this data alone. In passing, we note that it was found by Alvarez et al. [33], and it is also clear from Fig. 11 of [36], that $v_{\rm ph}$ and s are parallel in these heated wire experiments, so that the structures which to the eye look like sources, are *indeed* sources according to our definition.

In the coupled CGL equations ((2) and (3)), s_0 is the *linear* group velocity, i.e., the group velocity of the fast modes [3]. It is important to realize [68,69] that for positive ε, the group velocity s is *different* from s_0. To see this, note that the coupled CGL equations admit single mode traveling waves of the form

$$A_{\rm R} = a{\rm e}^{-{\rm i}(\omega_{\rm R}t-qx)}, \quad A_{\rm L} = 0, \tag{6}$$

or

$$A_{\rm L} = a{\rm e}^{-{\rm i}(\omega_{\rm L}t-qx)}, \quad A_{\rm R} = 0. \tag{7}$$

Substitution of these wave solutions in the amplitude equations ((2) and (3)) yields the nonlinear dispersion relation

$$\omega_{\rm R,L} = \pm s_0 q + (c_1 + c_3)q^2, \tag{8}$$

so that the group velocity $s = \partial\omega/\partial q$ of these traveling waves becomes

$$s_{\rm R} = s_{0,\rm R} + 2(c_1 + c_3)q, \quad \text{with } s_{0,\rm R} = s_0, \tag{9}$$

$$s_{\rm L} = s_{0,\rm L} + 2(c_1 + c_3)q, \quad \text{with } s_{0,\rm R} = -s_0. \tag{10}$$

When $\varepsilon \downarrow 0$, the band of the allowed q values shrinks to zero, and s approaches the linear group velocity $\pm s_0$, as it should. The term $2(c_1 + c_3)q$ accounts for the change in the group velocity away from threshold where the total wave number may differ from the critical value $q_{\rm c}$. This term involves both the linear and the nonlinear dispersion coefficient, and its importance increases with increasing ε. We will therefore sometimes refer to s as the *nonlinear* or *total* group velocity, to emphasize the difference between s_0 and s.

Clearly it is possible, that s_0 and s have opposite signs. Since the labels R and L of $A_{\rm R}$ and $A_{\rm L}$ refer to the signs of *linear* group velocity s_0, if this occurs, the mode $A_{\rm R}$ corresponds to a wave whose total group velocity s is to the left! The various possibilities concerning sources and sinks are illustrated in Fig. 1.

It is important to stress that our analysis focuses on sources and sinks near the primary supercritical Hopf bifurcation from a homogeneous state to traveling waves. Experimentally, sources and sinks have been studied in detail by Kolodner [37] in his experiments on traveling waves in binary mixtures. Unfortunately, for this system a direct comparison between theory and experiments is hindered by the fact that the transition to traveling waves is *subcritical*, not supercritical.

[3] We stress that the indices R and L of the amplitudes $A_{\rm R}$ and $A_{\rm L}$ are associated with the sign of the *linear group velocity* s_0. In writing Eq. (1) with $q_{\rm c}$ and $\omega_{\rm c}$ positive, we have also associated a wave whose phase velocity $v_{\rm ph}$ is to the right with $A_{\rm R}$, and one whose $v_{\rm ph}$ is to the left with $A_{\rm L}$, but this choice is completely arbitrary: At the level of the amplitude equations, the sign of the phase velocity of the critical mode plays no role.

3. Coherent structures; counting arguments for sources and sinks

3.1. Counting arguments: general formulations and summary of results

Many patterns that occur in experiments on traveling wave systems or numerical simulations of the single and coupled CGL equations (2) and (3) exhibit local structures that have an essentially time-independent shape and propagate with a constant velocity v. For these so-called *coherent* structures, the spatial and temporal degrees of freedom are not independent: apart from a phase factor, they are stationary in the co-moving frame $\xi = x - vt$. Since the appropriate functions that describe the profiles of these coherent structures depend only on the single variable ξ, these functions can be determined by ordinary differential equations (ODE's). These are obtained by substitution of the appropriate Ansatz in the original CGL equations, which of course are partial differential equations. Since the ODE's can themselves be written as a set of first order flow equations in a simple phase space, the coherent structures of the amplitude equations correspond to certain orbits of these ODE's. Please note that plane waves, since they have constant profiles, are trivial examples of coherent structures; in the flow equations they correspond to fixed points. Sources and sinks connect, asymptotically, plane waves, and so the corresponding orbits in the ODE's connect fixed points. Many different coherent structures have been identified within this framework [67–72].

The counting arguments that give the multiplicity of such solutions are essentially based on determining the dimensions of the stable and unstable manifolds near the fixed points. These dimensions, together with the parameters of the Ansatz such as v, determine for a certain orbit the number of constraints and the number of free parameters that can be varied to fullfill these constraints. We may illustrate the theoretical importance of counting arguments by recalling that for the single CGL equation a continuous family of hole solutions has been known to exist for some time [70]. Later, however, counting arguments showed that these source type solutions were on general grounds expected to come as discrete sets, not as a continuous one-parameter family [68,69]. This suggested that there is some accidental degeneracy or hidden symmetry in the single CGL equation, so that by adding a seemingly innocuous perturbation to the CGL equation, the family of hole solutions should collapse to a discrete set. This was indeed found to be the case [73,74]. For further details of the results and implications of these counting arguments for coherent structures in the single CGL equation, we refer to [68,69].

It should be stressed that counting arguments cannot prove the existence of certain coherent structures, nor can they establish the dynamical relevance of the solutions. They can only establish the multiplicity of the solutions, assuming that the equations have no hidden symmetries. Imagine that we know – either by an explicit construction or from numerical experiments – that a certain type of coherent structure solution does exist. The counting arguments then establish whether this should be an isolated or discrete solution (at most a member of a discrete set of them), or a member of a one-parameter family of solutions, etc. In the case of an isolated solution, there are no nearby solutions if we change one of the parameters (like the velocity v) somewhat. For a one-parameter family, the counting argument implies that when we start from a known solution and change the velocity, we have enough other free parameters available to make sure that there is a perturbed trajectory that flows into the proper fixed point as $\xi \to \infty$.

For the two coupled CGL equations (2) and (3) the counting can be performed by a straightforward extension of the counting for the single CGL equation [68,69]. The Ansatz for coherent structures of the coupled CGL equations (2) and (3) is the following generalization of the Ansatz for the single CGL equation

$$A_{\mathrm{L}}(x,t) = \mathrm{e}^{-\mathrm{i}\omega_{\mathrm{L}}t}\hat{A}_{\mathrm{L}}(x-vt), \quad A_{\mathrm{R}}(x,t) = \mathrm{e}^{-\mathrm{i}\omega_{\mathrm{R}}t}\hat{A}_{\mathrm{R}}(x-vt). \tag{11}$$

Note that we take the velocities of the structures in the left and right mode equal, while the frequencies ω are allowed to be different. This is due to the form of the coupling of the left-and right-traveling modes, which is through the moduli of the amplitudes. It obviously does not make sense to choose the velocities of the A_{L} and A_{R} differently: for large times the cores of the structures in A_{L} and A_{R} would then get arbitrarily far apart, and at the technical

level, this would be reflected by the fact that with different velocities we would not obtain simple ODE's for $\hat{A}_{\mathrm{L}}$ and $\hat{A}_{\mathrm{R}}$. Since the phases of A_{L} and A_{R} are not directly coupled, there is no a priori reason to take the frequencies ω_{L} and ω_{R} equal; in fact we will see that in numerical experiments they are not always equal (see for instance the simulations presented in Fig. 3). Allowing $\omega_{\mathrm{L}} \neq \omega_{\mathrm{R}}$, the Ansatz (11) clearly has three free parameters, ω_{L}, ω_{R} and v.

Substitution of the Ansatz (11) into the coupled CGL equations (2) and (3) yields the following set of ODE's:

$$\partial_\xi a_{\mathrm{L}} = \kappa_{\mathrm{L}} a_{\mathrm{L}}, \tag{12}$$

$$\partial_\xi z_{\mathrm{L}} = -z_{\mathrm{L}}^2 + \frac{1}{1+\mathrm{i}c_1}[-\varepsilon - \mathrm{i}\omega_{\mathrm{L}} + (1-\mathrm{i}c_3)a_{\mathrm{L}}^2 + g_2(1-\mathrm{i}c_2)a_{\mathrm{R}}^2 - (v+s_0)z_{\mathrm{L}}], \tag{13}$$

$$\partial_\xi a_{\mathrm{R}} = \kappa_{\mathrm{R}} a_{\mathrm{R}}, \tag{14}$$

$$\partial_\xi z_{\mathrm{R}} = -z_{\mathrm{R}}^2 + \frac{1}{1+\mathrm{i}c_1}[-\varepsilon - \mathrm{i}\omega_{\mathrm{R}} + (1-\mathrm{i}c_3)a_{\mathrm{R}}^2 + g_2(1-\mathrm{i}c_2)a_{\mathrm{L}}^2 - (v-s_0)z_{\mathrm{R}}], \tag{15}$$

where we have written

$$\hat{A}_{\mathrm{L}} = a_{\mathrm{L}} \mathrm{e}^{\mathrm{i}\phi_{\mathrm{L}}}, \quad \hat{A}_{\mathrm{R}} = a_{\mathrm{R}} \mathrm{e}^{\mathrm{i}\phi_{\mathrm{R}}}. \tag{16}$$

and where q, κ and z are defined as

$$q := \partial_\xi \phi, \quad \kappa := (1/a)\partial_\xi a, \quad z := \partial_\xi \ln(\hat{A}) = \kappa + \mathrm{i}q. \tag{17}$$

Compared to the flow equations for the single CGL equation (see Appendix A), there are two important differences that should be noted: (i) Instead of the velocity v we now have velocities $v \pm s_0$; this is simply due to the fact that the linear group velocity terms cannot be transformed away. (ii) The nonlinear coupling term in the CGL equations shows up only in the flow equations for the z's.

The fixed points of these flow equations, the points in phase space at which the right-hand sides of Eqs. (12)–(15) vanish, describe the asymptotic states for $\xi \to \pm\infty$ of the coherent structures. What are these fixed points? From Eq. (12) we find that either a_{L} or κ_{L} is equal to zero at a fixed point, and similarly, from Eq. (14) it follows that either a_{R} or κ_{R} vanishes. For the sources and sinks of (2) and (3) that we wish to study, the asymptotic states are left- and right-traveling waves. Therefore the fixed points of interest to us have either both a_{L} and κ_{R} or both a_{R} and κ_{L} equal to zero, and we search for heteroclinic orbits connecting these two fixed points.

As explained before, with counting arguments one determines the multiplicity of the coherent structures from (i) the dimension $\mathcal{D}^-_{\mathrm{out}}$ of the outgoing ("unstable") manifold of the fixed point describing the state on the left ($\xi = -\infty$), (ii) the dimension $\mathcal{D}^+_{\mathrm{out}}$ of the outgoing manifold at the fixed point characterizing the state on the right ($\xi = \infty$) and (iii) the number $\mathcal{N}_{\mathrm{free}}$ of free parameters in the flow equations. Note that every flowline of the ODE's corresponds to a particular coherent solution, with a fully determined spatial profile but with an *arbitrary* position; if we would also specify the point $\xi = 0$ on the flowline, the position of the coherent structure would be fixed. When we refer to the multiplicity of the coherent solutions, however, we only care about the profile and not the position. We therefore need to count the multiplicity of the *orbits*. In terms of the quantities given above, one thus expects a $(\mathcal{D}^-_{\mathrm{out}} - 1 - \mathcal{D}^+_{\mathrm{out}} + \mathcal{N}_{\mathrm{free}})$-parameter family of solutions; the factor -1 is associated with the invariance of the ODE's with respect to a shift in the pseudo-time ξ which leaves the flowlines invariant. In terms of the coherent structures, this symmetry is the translational invariance of the amplitude equations.

When the number $(\mathcal{D}^-_{\mathrm{out}} 1 - \mathcal{D}^+_{\mathrm{out}} + \mathcal{N}_{\mathrm{free}})$ is zero, one expects a discrete set of solutions, while if this number is negative, one expects there to be no solutions at all, generically. *Proving* the existence of solutions, within the context of an analysis of this type, amounts to proving that the outgoing manifold at the $\xi = -\infty$ fixed point and

the incoming manifold at the $\xi = \infty$ fixed point intersect. Such proofs are in practice far from trivial – if at all possible – and will not be attempted here.

Conceptually, counting arguments are simple, since the dimensions $\mathcal{D}^{-}_{\mathrm{out}}$ and $\mathcal{D}^{+}_{\mathrm{out}}$ are just determined by studying the linear flow in the neighborhood of the fixed points. Technically, the analysis of the coupled equations is a straightforward but somewhat involved extension of the earlier findings for the single CGL. We therefore prefer to only quote the main result of the analysis, and to relegate all technicalities to Appendix B.

For sources and sinks, always one of the two modes vanishes at the relevant fixed points. We are especially interested in the case in which the effective value of ε, defined as

$$\varepsilon^{\mathrm{L}}_{\mathrm{eff}} := \varepsilon - g_2|a_{\mathrm{R}}|^2, \qquad \varepsilon^{\mathrm{R}}_{\mathrm{eff}} := \varepsilon - g_2|a_{\mathrm{L}}|^2. \tag{18}$$

is *negative* for the mode which is suppressed. In this case small perturbations of the suppressed mode decay to zero in each of the single-amplitude domains, so this situation is then *stable*. E.g., for a stable source configuration as sketched in Fig. 2, $\varepsilon^{\mathrm{R}}_{\mathrm{eff}}$ should be negative on the left, and $\varepsilon^{\mathrm{L}}_{\mathrm{eff}}$ should be negative on the right of the source. We will focus on the results for this regime of full suppression of one mode by the other.

The basic result of our counting analysis for the multiplicity of source and sink solutions is that when $\varepsilon_{\mathrm{eff}} < 0$ the counting arguments for *"normal"* sources and sinks (the linear group velocity s_0 and the nonlinear group velocity s of the same sign), is simply that

- *Sources occur in discrete sets. Within these sets, as a result of the left–right symmetry for $v = 0$, we expect a stationary, symmetric source to occur.*
- *Sinks occur in a two-parameter family.*

Notice that apart from the conditions formulated above, these findings are completely independent of the precise values of the coefficients of the equations. This gives these results their predictive power. Essentially all of the results of the remainder of this paper are based on the first finding that sources come in discrete sets, so that they fix the properties of the states in the domains they separate.

As discussed in Appendix B the multiplicity of *anomalous* sources is the same as for normal sources and sinks in large parts of parameter space, but larger multiplicities *can* occur. Likewise, sources with $\varepsilon_{\mathrm{eff}} > 0$ may occur as a two-parameter family, although most of these are expected to be unstable (Section B.7). We shall see in Section 5 that in this case, which happens especially when g_2 is only slightly larger than 1, new nontrivial dynamics can occur.

3.2. Comparison between shooting and direct simulations

Clearly, the coherent structure solutions are by construction *special* solutions of the original partial differential equations. The question then arises whether these solutions are also dynamically relevant, in other words, whether they emerge naturally in the long time dynamics of the CGL equation or as "nearby" transient solutions in nontrivial dynamical regimes. For the single CGL equation, this has indeed been found to be the case [67–69,75–80]. To check that this is also the case here, we have performed simulations of the coupled CGL equations and compared the sinks and sources that are found there to the ones obtained from the ODE's (12)–(15). Direct integration of the coupled CGL equations was done using a pseudo-spectral code. The profiles of uniformly translating coherent structures were obtained by direct integration of the ODE's (12)–(15), shooting from both the $\xi = +\infty$ and $\xi = -\infty$ fixed points and matching in the middle.

In Fig. 2(a), we show a space–time plot of the evolution towards sources and sinks, starting from random initial conditions. The grey shading is such that patches of A_{R} mode are light and A_{L} mode are dark. Clearly, after a quite short transient regime, a stationary sink/source pattern emerges. In Fig. 2(b) we show the amplitude profiles of $|A_{\mathrm{R}}|$ (thin curve) and $|A_{\mathrm{L}}|$ (thick curve) in the final state of the simulations that are shown in Fig. 2(a). In

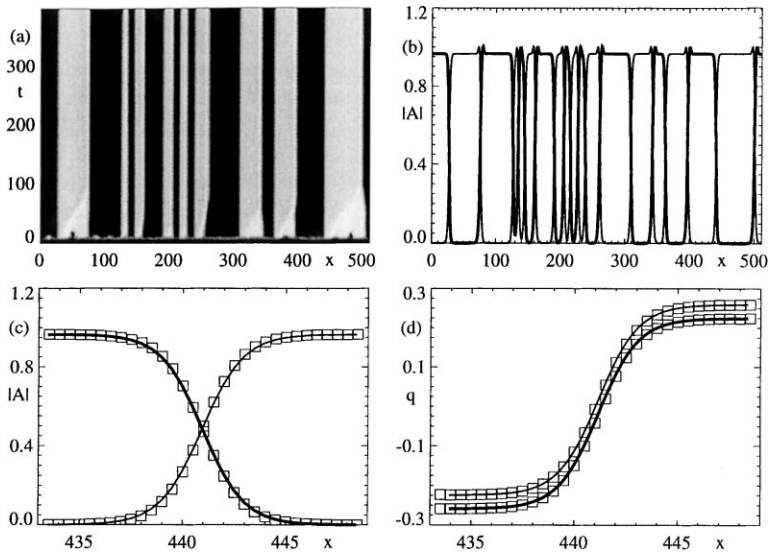

Fig. 2. (a) Space–time plot showing the evolution of the amplitudes $|A_L|$ and $|A_R|$ in the CGL equations starting from random initial conditions. The coefficients were chosen as $c_1 = 0.6$, $c_2 = 0.0$, $c_3 = 0.4$, $s_0 = 0.4$, $g_2 = 2$ and $\varepsilon = 1$. The grey shading is such that patches of A_R mode are light and the A_L mode are dark. (b) Amplitude profiles of the final state of (a), showing a typical sink/source pattern. (c) Comparison between the source obtained from direct simulations of the CGL equations as shown in (b) (squares) and profiles obtained by shooting in the ODE's (12)–(15) (full curves). (d) Similar comparison, now for the wavenumber profiles. In (c) and (d), the thick (thin) curves correspond to the left (right) traveling mode.

Fig. 2(c) and (d) we compare the amplitude and wavenumber profile of the source obtained from the CGL equations around $x = 440$ (boxes) to the source that is obtained from the ODE's (12)–(15) (full lines). The fit is excellent, which illustrates our finding that sources are stable and stationary in large regions of parameter space and that their profile is completely determined by the ODE's associated with the Ansatz (11).

However, the CGL equations posses a large number of coefficients that can be varied, and it will turn out that there are several mechanisms that can render sources and source/sink patterns unstable. We will encounter these scenarios in Sections 4 and 5.

3.3. Multiple discrete sources

As we already pointed out before, the fact that sources come in a discrete set does not imply that there exists only one unique source solution. There could in principle be more solutions, since the counting only tells us that infinitesimally close to any given solution, there will not be another one.

Fig. 3 shows an example of the occurrence of two different isolated source solutions. The figure is a space–time plot of a simulation where we obtained two different sources, one of which is an anomalous one (s and s_0 of opposite sign). One clearly sees the different wavenumbers emitted by the two structures, and sandwiched in between these two sources is a single amplitude sink, whose velocity is determined by the difference in incoming wavenumbers. We have checked that the wavenumber selected by the anomalous source is such that the counting still yields a discrete set. If we follow the spatio-temporal evolution of this particular configuration, we find highly nontrivial behavior which we do not fully understand as of yet (not shown in Fig. 3).

These findings illustrate our belief that the "normal" sources and sinks are the most relevant structures one expects to encounter. It therefore appears to be safe to ignore the possible dynamical consequences of the more esoteric structures, which one a priori cannot rule out. The main complication of the possible occurrence of multiple discrete

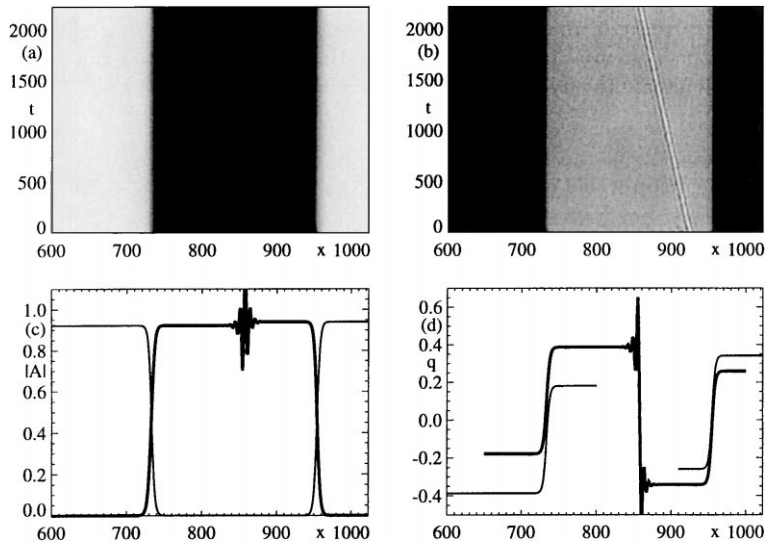

Fig. 3. (a,b) Space–time plots showing $|A_R|$ (a) and $|A_L|$ (b) in a situation in which there are two different sources present. Coefficients in this simulation are $c_1 = 3.0$, $c_2 = 0$, $c_3 = 0.75$, $g_2 = 2.0$, $s_0 = 0.2$ and $\varepsilon = 1.0$. Initial conditions were chosen such that a well-separated source-source pair emerges, and a short transient has been removed. The source at $x \approx 730$ is anomalous, i.e., its linear and nonlinear group velocity s_0 and s have opposite signs. Sandwiched between the sources is a single-mode sink, traveling in the direction of the anomalous source; this sink is visible in (b). (c) Snapshot of the amplitude profiles of the two sources and the single mode sink at the end of the simulation shown in (a-b). (d) The wavenumber profiles of the two sources in their final state. Note that when the modulus goes to zero, the wavenumber is no longer well-defined; we can only obtain q up to a finite distance from the sources. The selected wavenumber emitted by the anomalous source is $q_{sel} = 0.387$, while the wavenumber emitted by the ordinary source is $q_{sel} = 0.341$. The velocity of the sink in between agrees with the velocity that follows from a phase-matching rule, i.e., the requirement that the phase difference across the sink remains constant. In (c) and (d), thick (thin) curves correspond to left (right) traveling modes.

sources, as in Fig. 3, is that single amplitude sinks can arise in the patches separating them. The motion of these sinks can dominate the dynamics for an appreciable time.

4. Scaling properties of sources and sinks for small ε

In this section we study the scaling properties and dynamical behavior of sources and sinks in the limit where ε is small. This is a nontrivial issue, since due to the presence of the linear group velocity s_0, the coupled CGL equations do not scale uniformly with ε. We focus in particular on the width of the sources and sinks. The results we obtain are open for experimental testing, since the control parameter ε can usually be varied quite easily. The behavior of the sources is the most interesting, and we will discuss this in Sections 4.1 and 4.2. Using arguments from the theory of front propagation, we recover the result from Coullet et al. [48] that there is a finite threshold value for ε, below which no *coherent* sources exist (Section 4.1). For ε below this critical value, there are, depending on the initial conditions, roughly two different possibilities. For well-separated sink/source patterns, we find *non-stationary* sources whose average width scales as $1/\varepsilon$ (in possible agreement with the experiments of Vince and Dubois [35]; see Section 6.2.1). These sources can exist for arbitrarily small values of ε. For patterns with less-well separated sources and sinks, we typically find that the sources and sinks annihilate each other and disappear altogether. The system evolves then to a single mode state, as described by the averaged amplitude equations (4) and (5). These scenarios are discussed in Section 4.2. By some simple analytical arguments we obtain that the width of coherent sinks diverges as $1/\varepsilon$; typically these structures remain stationary (see Section 4.3).

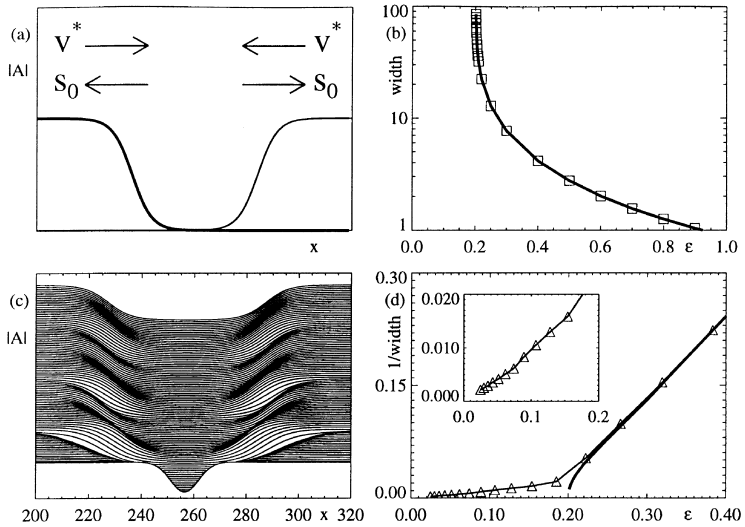

Fig. 4. (a) Sketch of a wide source, indicating the competition between the linear group velocity s_0 and the front velocity v^*. (b) Width of coherent sources as obtained by shooting, for $c_1 = c_3 = 0.5$, $c_2 = 0$, $g_2 = 2$ and $s_0 = 1$. (c) Example of dynamical source for same values of the coefficients and $\varepsilon = 0.15$. The order parameter shown here is the sum of the amplitudes $|A_L|$ and $|A_R|$, and the total time shown here is 1000. (d) Average inverse width of sources for the same coefficients as (b) as a function of ε. The thick curve corresponds to the coherent sources as shown in (b). For ε close to and below $\varepsilon_c^{so} = 0.2$, there is a crossover to dynamical behavior. The inset shows the region around $\varepsilon = 0$, where the average width roughly scales as ε^{-1}.

4.1. Coherent sources: analytical arguments

By balancing the linear group velocity term with the second order spatial derivative terms, we see that the coupled amplitude equations (2) and (3) may contain solutions whose widths approach a finite value of order $1/s_0$ as $\varepsilon \to 0$. As pointed out in particular by Cross [26,27], this behavior might be expected near end walls in finite systems; in principle, it could also occur for coherent structures such as sources and sinks which connect two oppositely traveling waves. Solutions of this type are *not* consistent with the usual assumption of separation of scales (length scale $\sim \varepsilon^{-1/2}$) which underlies the derivation of amplitude equations. One should interpret the results for such solutions with caution.

As we shall discuss, the existence of stationary, coherent sources is governed by a finite critical value ε_c^{so}, first identified by Coullet et al. [48]. Since the coupled amplitude equations (2) and (3) are only valid to lowest order in ε, the question then arises whether the existence of this finite critical values ε_c^{so} is a peculiarity of the lowest order amplitude equations. Since this threshold is determined by the interplay of the linear group velocity and a front velocity, which are both defined for arbitrary ε, we will argue that the existence of a threshold is a robust property indeed.

We now proceed by deriving this critical value ε_c^{so} from a slightly different perspective than the one that underlies the analysis of Coullet et al. [48], by viewing wide sources as weakly bound states of two widely separated fronts. Indeed, consider a sufficiently wide source like the one sketched in Fig. 4(a) in which there is quite a large interval where both amplitudes are close to zero [4]. Intuitively, we can view such a source as a weakly bound state of two fronts, since in the region where one of the amplitudes crosses over from nearly zero to some value of order unity,

[4] It is not completely obvious that wide sources necessarily have such a large zero patch, but this is what we have found from numerical simulations. Wide sinks actually will turn out not to have this property.

the other mode is nearly zero. Hence as a first approximation in describing the fronts that build up the wide source of the type sketched in Fig. 4(a), we can neglect the coupling term proportional to g_2 in the core-region. The resulting fronts will now be analyzed in the context of the single CGL equation.

Let us look at the motion of the A_R front on the right (by symmetry the A_L front travels in the opposite direction). As argued above, its motion is governed by the single CGL equation in a frame moving with velocity s_0

$$(\partial_t + s_0\partial_x)A_R = \varepsilon A_R + (1 + ic_1)\partial_x^2 A_R - (1 - ic_3)|A_R|^2 A_R. \tag{19}$$

The front that we are interested in here corresponds to a front propagating "upstream", i.e., to the left, into the *unstable* $A_R = 0$ state. Such fronts have been studied in detail [68,69], both in general and for the single CGL equation specifically.

Fronts propagating into unstable states come in two classes, depending on the nonlinearities involved. Typically, when the nonlinearities are saturating, as in the cubic CGL equation (19), the asymptotic front velocity v_{front} equals the *linear spreading velocity* v^*. This v^* is the velocity at which a small perturbation around the unstable state grows and spreads according to the *linearized* equations. For Eq. (19), the velocity v^* of the front, propagating into the unstable $A = 0$ state, is given by [68,69]

$$v^* = s_0 - 2\sqrt{\varepsilon(1 + c_1^2)}. \tag{20}$$

The parameter regime in which the selected front velocity is v^* is often referred to as the "linear marginal stability" [81–85] or "pulled fronts" [86–89] regime, as in this regime the front is "pulled along" by the growing and spreading of linear perturbations in the tip of the front.

For small ε, the velocity $v^* = v_{\text{front}}$ is positive, implying that the front moves to the right, while for large ε, v^* is negative so that the front moves to the left. Intuitively, it is quite clear that the value of ε where $v^* = 0$ will be an important critical value for the dynamics, since for larger ε the two fronts sketched in Fig. 4(a) will move towards each other, and some kind of source structure is bound to emerge. For $\varepsilon < \varepsilon_c^{so}$, however, there is a possibility that a source splits up into two retracting fronts. Hence the critical value of ε is defined through $v^*(\varepsilon_c^{so}) = 0$, which, according to Eq. (20) yields

$$\varepsilon_c^{so} = s_0^2/(4 + 4c_1^2). \tag{21}$$

We will indeed find that the width of *coherent* sources diverges for this value of ε; however, the sources will not disappear altogether, but are replaced by *non-stationary* sources which cannot be described by the coherent structures Ansatz (11).

4.2. Sources: numerical simulations

By using the shooting method, i.e., numerical integration of the ODE's (12)–(15), to obtain coherent sources, we have studied the width of the coherent sources as a function of ε. The width is defined here as the distance between the two points where the left and right traveling amplitudes reach 50% of their respective asymptotic values. In Fig. 4(b), we show how the width of coherent sources varies with ε. For the particular choice of coefficients here ($c1 = c_3 = 0.5$, $c_2 = 0$, $g_2 = 2$ and $s_0 = 1$), $\varepsilon_c^{so} = 0.2$, and it is clear from this figure, that the width of stationary source solutions of Eq. (19) diverges at this critical value [5].

In dynamical simulations of the full coupled CGL equations however, this divergence is cut off by a crossover to the dynamical regime characteristic of the $\varepsilon < \varepsilon_c^{so}$ behavior. Fig. 4(c) is a space–time plot of $|A_L| + |A_R|$ that

[5] Note that by a rescaling of the CGL equations, one can set $s_0 = 1$ without loss of generality.

illustrates the incoherent dynamics we observe for $\varepsilon < \varepsilon_c^{so}$. The initial condition here is source-like, albeit with a very small width. In the simulation shown, we see the initial source flank diverge as we would expect since $s_0 > v^*$. As time progresses, right ahead of the front a small 'bump' appears: as we mentioned before, both amplitudes are to a very good approximation zero in that region, so the state there is unstable (remember that though small, ε is still nonzero). This bump will therefore start to grow, and will be advected in the direction of the flank. The flank and bump then merge and the flank jumps forward. The average front velocity is thus enhanced. The front then slowly retracts again, and the process is repeated, resulting in a "breathing" type of motion. For longer times these oscillations become very, very small. For this particular choice of parameters, they become almost invisible after times of the order 3000; however, a close inspection of the data yields that the sources never become stationary but keep performing irregular oscillations. Since these fluctuations are so small, it is very likely that to an experimentalist such sources appear to be completely stationary.

From the point of view of the stability of sources, we can think of the change of behavior of the sources as a core-instability. This instability is basically triggered by the fact that wide sources have a large core where both A_L and A_R are small, and since the neutral state is unstable, this renders the sources unstable. The difference between the critical value of ε where the instability sets in and ε_c^{so} is minute, and we will not dwell on the distinction between the two [6]. Although all our numerical results are in accord with this scenario, one should be aware, however, that it is not excluded that other types of core-instabilities exist in some regions of parameter space [7]. Furthermore, it should be pointed out that when ε is below ε_c^{so}, there is *no* stationary albeit unstable source! The dynamical sources can than *not* be viewed as oscillating around an unstable stationary source.

The weak fluctuations of the source flanks are very similar to the fluctuations of domain walls between single and bimodal states in inhomogeneously coupled CGL equations as studied in [66]. Completely analogous to what is found here, there is a threshold given in terms of ε and s_0 for the existence of stationary domain walls, which we understand now to result from a similar competition between fronts and linear group velocities. Beyond the threshold, dynamical behavior was shown to set in, which, depending on the coefficients, can take qualitatively different forms; similar scenarios can be obtained for the sources here.

The main ingredient that generates the dynamics seems to be the following. For a very wide source, we can think of the flank of the source as an isolated front. However, the *tip* of this front will always feel the other mode, and it is precisely this tip which plays an essential role in the propagation of "pulled" fronts [81–83,86–89]! Close inspection of the numerics shows that near the crossover between the front regime and the interaction regime, oscillations, phase slips or kinks are generated, which are subsequently advected in the direction of the flank. These perturbations are a *deterministic* source of perturbations, and it is these perturbations that make the flank jump forward, effectively narrowing down the source.

The jumping forward of the flank of the source for ε just below ε_c^{so} is reminiscent to the mechanism through which traveling pulses were found to acquire incoherent dynamical behavior, if their velocity was different from the linear group velocity [93]. In extensions of the CGL equation, it was found that if a pulse would travel slower than the linear spreading speed v^*, fluctuations in the region just ahead of the pulse could grow out and make the pulse at one point "jump ahead". In much the same way the fronts can be viewed to "jump ahead" in the wide source-type structures below ε_c^{so} when the fluctuations ahead of it grow sufficiently large.

[6] For a similar scenario in the context of non-homogeneously coupled CGL equations, see [66].

[7] An example of a similar scenario is provided by pulses in the single quintic CGL equation. Pulses are structures consisting of localized regions where $|A| \neq 0$. The existence and stability of pulse solutions can, to a large extent, be understood by thinking of a pulse as a bound state of two fronts [68,69]. However, recent perturbative calculations near the non-dissipative (Schrödinger-like) limit [90–92] have shown that in some parameter regimes a pulse can become unstable against a localized mode. This particular instability can not simply be understood by viewing a pulse as a bound state of two fronts.

In passing, we point out that we believe these various types of "breathing dynamics" to be a general feature of the interaction between local structures and fronts. Apart from the examples mentioned above, a well known example of incoherent local structures are the oscillating pulses observed by Brand and Deissler in the quintic CGL [94,95]. Also in this case we have found that these oscillations are due to the interaction with a front, but instead of a pulled front it is a *pushed* front that drives the oscillations here [96].

Returning to the discussion of the behavior of the wide non-stationary sources, we show in Fig. 4(d) the (inverse) average width of the dynamical sources for small ε. These simulations were done in a large system (size 2048), with just one source and, due to the periodic boundary conditions, one sink. If one slowly decreases ε, one finds that the average width of the sources diverges roughly as ε^{-1} (see the inset of Fig. 4(d)). However, if one does not take such a large system, i.e., sources and sinks are not so well separated, we often observed that, after a few oscillations of the sources, they interact with the sinks and annihilate. In many cases, especially for small enough ε, *all* sources and sinks disappear from the system, and one ends up with a state of only right or left traveling wave. Since no sources or sinks can occur in the average equations (4) and (5), this behavior seems precisely to be what these average equations predict. In a sense, this regime without sources and sinks follow nicely from the ordinary CGL equations when $\varepsilon \downarrow 0$.

In conclusion, we arrive at the following scenario:

- For $\varepsilon > \varepsilon_c^{so}$, sources are *stationary* and stable, provided that the waves they send out are stable. The structure of these stationary source solutions is given by the ODE's (12)–(15), and their multiplicity is determined by the counting arguments.
- When $\varepsilon \downarrow \varepsilon_c^{so}$, the source width rapidly increases, and for $\varepsilon = \varepsilon_c^{so}$, the size of the coherent sources (i.e., solutions of the ODE's (12)–(15)) diverges, in agreement with the picture of a source consisting of two weakly bound fronts. For a value of ε just above ε_c^{so}, the sources have a wide core where both A_R and A_R are close to zero, and these sources turn unstable. Our scenario is that in this regime a source consists essentially of two of the "nonlinear global modes" of Couairon and Chomaz [97]. Possibly, their analysis can be extended to study the divergence of the source width as $\varepsilon \downarrow \varepsilon_c^{so}$.
- For $\varepsilon < \varepsilon_c^{so}$, *wide*, *non-stationary* sources can exist. Their dynamical behavior is governed by the continuous emergence and growth of fluctuations in the region where both amplitudes are small, resulting in an incoherent "breathing" appearance of the source. For long times, these oscillations may become very mild, especially when ε is not very far below ε_c^{so}.
- In the limit for $\varepsilon \downarrow 0$, there are, depending on the initial conditions, two possibilities. For random initial conditions, pairs of sources and sinks annihilate and the system often ends up in a single mode state, which is consistent with the 'averaged equation' picture discussed in Section 1.2.2. This happens in particular in sufficiently small systems. Alternatively, in large systems, one may generate well-separated sources and sinks. In this case the average width of the incoherent sources diverges as $1/\varepsilon$, in apparent agreement with the experiments of Vince and Dubois [35] (see Section 6.2.1 for further discussion of this point).

We finally note that our discussion above was based on the fact that near a supercritical bifurcation, fronts propagating into an unstable state are "pulled" [86–89] or "linear marginal stability" [81–85] fronts: $v_{front} = v^*$. It is well-known that when some of the nonlinear terms tend to enhance the growth of the amplitude, the front velocity can be higher: $v_{front} > v^*$ [81–89]. These fronts, which occur in particular near a subcritical bifurcation, are sometimes called "pushed" [86–89] or "nonlinearly marginal stability" [68,69,85] fronts. In this case it can happen that the front velocity remains large enough for stable stationary sources to exist all the way down to $\varepsilon = 0$. We believe that this is probably the reason that Kolodner [38] does not appear to have seen any evidence for the existence of a critical ε_c^{so} in his experiments on traveling waves in binary mixtures, as in this system the transition is weakly subcritical [21,98].

4.3. Sinks

As we have seen in Section B.2, counting arguments show that there generically exists a two-parameter family of uniformly translating sink solutions. The scaling of their width as a function of ε is not completely obvious, since the figures of Cross [26] [8] indicate that their width approaches a finite value as $\varepsilon \downarrow 0$, while Coullet et al. found a class of sink solutions whose width diverges as ε^{-1} for $\varepsilon \downarrow 0$.

In Appendix C we demonstrate, by examining the ODE's (12)–(15) in the $\varepsilon \downarrow 0$ limit, that the asymptotic scaling of the width of sinks as ε^{-1} follows naturally.

If we now focus again on uniformly translating sink structures of the form

$$A_{\mathrm{R,L}} = \mathrm{e}^{-\mathrm{i}\omega_{\mathrm{R,L}} t}\, \hat{A}_{\mathrm{R,L}}(\xi), \tag{22}$$

and explicitly carry out this scaling by introducing the scaled variables

$$\bar{\xi} = \varepsilon\xi, \quad \bar{\omega}_{\mathrm{R,L}} = \frac{\omega_{\mathrm{R,L}}}{\varepsilon}, \quad \bar{A}_{\mathrm{R,L}} = \frac{\hat{A}_{\mathrm{R,L}}}{\sqrt{\varepsilon}}, \tag{23}$$

We find that, *if* the limit $\varepsilon \to 0$ is regular we can (to lowest order in ε), approximate the ODE's (12)–(15) by the following reduced set of equations

$$(-\mathrm{i}\bar{\omega} + s_0\partial_{\bar{\xi}})\bar{A}_{\mathrm{R}} = \bar{A}_{\mathrm{R}} - (1 - \mathrm{i}c_3)|\bar{A}_{\mathrm{R}}|^2\bar{A}_{\mathrm{R}} - g_2(1 - \mathrm{i}c_2)|\bar{A}_{\mathrm{L}}|^2\bar{A}_{\mathrm{R}}, \tag{24}$$

$$(-\mathrm{i}\bar{\omega} - s_0\partial_{\bar{\xi}})\bar{A}_{\mathrm{L}} = \bar{A}_{\mathrm{L}} - (1 - \mathrm{i}c_3)|\bar{A}_{\mathrm{L}}|^2\bar{A}_{\mathrm{L}} - g_2(1 - \mathrm{i}c_2)|\bar{A}_{\mathrm{R}}|^2\bar{A}_{\mathrm{L}}, \tag{25}$$

where we have set $\bar{\omega}_{\mathrm{R}} = \bar{\omega}_{\mathrm{L}} = \omega$ and $v = 0$, to study symmetric, stationary sinks. As one can see by comparing Eqs. (24) and (25) with the original Eqs. (12)–(15), the taking of the $\varepsilon \to 0$ limit effectively amounts to the removal of the diffusive term $\propto \partial_{\bar{\xi}}^2$. One could *a priori* wonder whether this procedure is justified, since we are removing the highest order derivative from the equations, which could very well constitute a singular perturbation. This matter will be resolved with the aid of our counting argument.

Eqs. (24) and (25) admit an exact solution for the sink profile, first obtained by Coullet et al. When we substitute

$$\bar{A}_{\mathrm{R,L}} = \bar{a}_{\mathrm{L}}\mathrm{e}^{\mathrm{i}\bar{\phi}_{\mathrm{R,L}}}, \quad \bar{q}_{\mathrm{R,L}} = \partial_{\bar{\xi}}\bar{\phi}_{\mathrm{R,L}}, \tag{26}$$

the explicit solution is given by

$$a_{\mathrm{R}}(x) = \sqrt{\frac{\varepsilon}{1 + \mathrm{e}^{(2(g_2-1)\varepsilon x)/s_0}}} = \sqrt{\varepsilon - a_{\mathrm{L}}^2}. \tag{27}$$

The width of these solutions is easily seen to indeed diverge as ε^{-1}. Since we can still vary $\bar{\omega}$ continuously to give various values for the asymptotic wavenumber, which is for solutions of the type (27) given by

$$\bar{q}_{\mathrm{R}} = \frac{1}{s_0}(\bar{\omega} + c_3) \text{ for } \bar{\xi} = -\infty \text{ and } \bar{q}_{\mathrm{L}} = \frac{-1}{s_0}(\bar{\omega} + c_3) \text{ for } \bar{\xi} = \infty, \tag{28}$$

we see that we still have a one-parameter family of $v = 0$ sinks. Since this is in accord with the full counting argument, the limit $\varepsilon \downarrow 0$ is indeed regular.

In passing we note that source solutions of finite width are completely absent in the scaled Eqs. (24) and (25). This is because the only orbit that starts from the $A_{\mathrm{R}} = 0$ single mode fixed point and flows to the $A_{\mathrm{L}} = 0$ single

[8] The work of Cross was motivated by experiments on traveling waves in binary mixtures. In such systems, the bifurcation is weakly subcritical; experimentally, the sinks width is then expected to be finite for small ε.

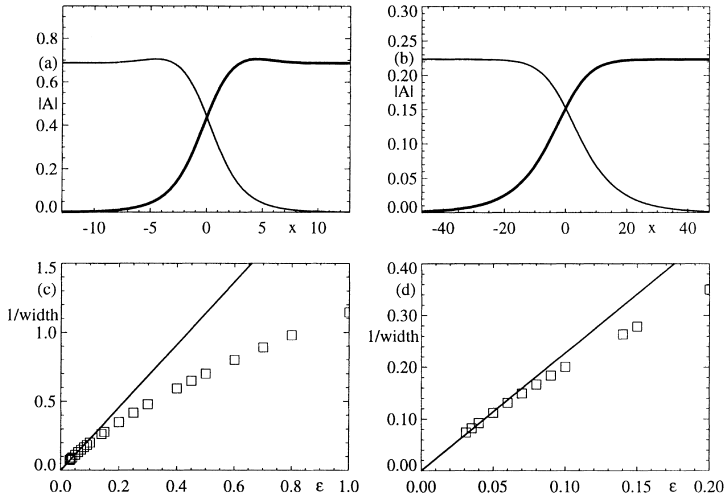

Fig. 5. The width of stationary sinks obtained from the ODE's Eqs. (12) and (15) as a function of ε, for $c_1 = 0.6$, $c_3 = 0.4$, $c_2 = 0$, $s_0 = 0.4$, $g_0 = 1$ and $g_2 = 2$. (a) Example of the stationary sink which has an incoming wavenumber corresponding to the wavenumber that is selected by the sources, for $\varepsilon = 0.5$. (b) *Idem*, now for $\varepsilon = 0.05$. Notice the differences in scale between (a) and (b). These two sinks are not related by simple scale transformations; this illustrates again the absence of uniform ε scaling of the coupled CGL equations. (c) As ε is decreased, the sink width initially roughly increases as $\varepsilon^{-1/2}$. When ε becomes sufficiently small, the group-velocity terms dominate over the diffusive/dispersive terms, and the sink-width is seen to obey an asymptotic ε^{-1} scaling (see (d) for a blowup around $\varepsilon = 0$. The straight line indicates the analytic result for the 50% width as obtained from Eq. (27), i.e. width$^{-1} = 5\varepsilon/(2\ln 3)$.

mode fixed point passes through the $A_L = A_R = 0$ fixed point, and therefore takes an infinite pseudo-time ξ; such a source has an infinitely wide core regime where A_L and A_R are both zero. This also agrees with our earlier observations, since the coherent sources already diverge at finite ε_c^{so}.

In Fig. 5 we plot the sink width versus ε for the full set of ODE's, as obtained from our shooting. It is clear that the sink indeed diverges at $\varepsilon = 0$, and that it asymptotically approaches the theoretical prediction from the above analysis.

4.4. *The limit* $s_0 \to 0$

In this paper, we focus mainly on the experimentally most relevant limit s_0 *finite*, ε *small*. For completeness, we also mention that Malomed [49] has also investigated the limit where ε is nonzero and $s_0 \to 0, c_i \to 0$, perturbatively. In this limit, which is relevant for some laser systems [60,61], sinks are found to be *wider* than sources. This finding can easily be recovered from the results of our appendix: from (A.12) it follows that to first order in s_0 the change in the exponential growth rate κ of the suppressed mode away from zero is

$$\delta\kappa_L^{\pm} = -s_0/2, \qquad \delta\kappa_R^{\pm} = s_0/2. \tag{29}$$

where according to our convention of the Appendices, κ^- corresponds to the negative root of (A.12), and κ^+ to the positive one. For a sink, the left traveling mode is suppressed on the left of the structure, and so this mode grows as $\exp(\kappa_L^+\xi)$, while on the right of the sink the right-traveling mode decays to zero as $\exp(\kappa_L^-\xi)$. For the sources, the right and left traveling modes are interchanged. According to (29), upon increasing s_0 the relevant rate of spatial growth and decay decreases for sinks and increases for sources. Hence in this limit, somewhat counter-intuitively, sinks are wider than sources. For a further discussion of the limit $s_0 \to 0$, we refer to the paper by Malomed [49].

Table 1
Overview of disordered and chaotic states

Type	Section	Figure	Parameters
Core-instabilities	4.1 and 4.2	4	$\varepsilon < \varepsilon_c^{so} = s_0^2/(4+4c_1^2)$
Absolute instabilities	5.1	7 and 8	$v_{BF}^* > 0$
Bimodal chaos	5.2	9	$1 < g_2 < \varepsilon/(\varepsilon - q_{sel})$
Defects+Bimodal	5.3.2	10	g_2 just above 1
Intermittent+Bimodal	5.3.3	11	g_2 just above 1
Periodic patterns	5.3.4	7,8 and 12	c_2,c_3: opposite signs and not small

5. Dynamical properties of source/sink patterns

Apart from the instability of the sources that occurs when $\varepsilon < \varepsilon_c^{so}$, there are at least two other mechanisms that lead to nontrivial dynamics of source/sink patterns, and this section is devoted to a description of such states. Due to the high dimensionality of the parameter space (one has to consider, in principle, the coefficients c_1, c_2, c_3, g_2 and ε or s_0), we aim at presenting some typical examples and uncovering general mechanisms, rather than aiming at a complete overview. Several of the scenario's we lay out deserve further detailed investigation in the future.

The starting point of our analysis here is the discrete nature of the sources (see Section B.2) which implies that the wavenumber of the laminar patches is often uniquely determined [47,49,51]. A stability analysis of these waves yields the two following instability mechanisms:

- Benjamin–Feir instability. When the waves emitted by the sources are unstable to long wavelength modes, it is the nature of this instability, i.e., whether it is *convective* or *absolute*, that determines the global dynamical behavior. The dynamical states that occur in this case are discussed in Section 5.1.
- Bimodal instabilities. The selected wavenumber can also lead to an instability resulting from the competition between the left and right traveling modes. The essential observation is that for a selected wavenumber q_{sel} there exists a range $1 < g_2 < \varepsilon/(\varepsilon - q_{sel}^2)$ for which *both* single and bimodal states are unstable. Provided that there are sources in the system, we find then a regime of *source-induced bimodal* chaos (see Section 5.2).

Furthermore, both of these instabilities can occur simultaneously, as seems to be the case in experiments of the Saclay group [40], and can be combined with the small-ε instability of the sources, discussed in Section 4. This leads to quite a rich palette of dynamical and chaotic states (Section 5.3). We have summarized the various disordered states that are typical for the coupled amplitude equations in Table 1. The first three types of dynamics are source-driven. Sources are not essential for the last three types of dynamics, which are driven by the coupling between the A_L and A_R modes.

5.1. Convective and absolute sideband-instabilities

Plane waves in the single CGL equation with wavenumber q exhibit sideband instabilities when [2] [9]

$$q^2 > \frac{\varepsilon(1-c_1c_3)}{3-c_1c_3+2c_3^2}, \tag{30}$$

[9] When both nominator and denominator are negative, as may occur for large c_1, this equation seems to suggest that one might have a stable band of wavenumbers. However, when $1-c_1c_3$ is negative, no waves are stable; the flipping of the sign of the denominator for large c_1 bears no physical relevance, but is due to a long-wavelength expansion performed to obtain Eq. (30). Note that the denominator is always positive as long as $1-c_1c_3$ is positive.

and when the curve $c_1c_3 = 1$ is crossed, all plane waves become unstable, and one encounters various types of spatio-temporal chaos [2,63–65]. For the coupled CGL equations under consideration here, the condition for linear stability of a single mode is still given by Eq. (30), since the mode which is suppressed is coupled quadratically to the one which is nonzero. Since the sources in general select a wavenumber unequal to zero, the relevant stability boundary for the plane waves in source/sink patterns typically lies below the $c_1c_3 = 1$ curve.

Consider now a linearly unstable plane wave. Perturbations of this wave grow, spread and are advected by the group velocity. The instability of the wave is called convective when the perturbations are advected away faster than they grow and spread; when monitored at a fixed position, all perturbations eventually decay. In the case of absolute instability, the perturbations spread faster than they are advected; such an instability often results in persistent dynamics. To distinguish between these two cases one has to compare, therefore, the group velocity and the spreading velocity of perturbations. For a general introduction to the concepts of convective and absolute instabilities, see e.g. [99,100].

Numerical simulations of the coupled CGL equations presented show that the distinction between the two types of instabilities is important for the dynamical behavior of the source/sink patterns. When the waves that are selected by the sources are convectively unstable, we find that, after transients have died out, the pattern typically "freezes" in an irregular juxtaposition of stationary sources and sinks. When the waves are absolutely unstable [10], however, persistent chaos occurs.

The wavenumber selection and instability scenario sketched above for the coupled CGL equations is essentially the one-dimensional analogue to the "vortex-glass" and defect chaos states in the 2D CGL equation [101–104]; in that case the wavenumber is selected by so-called spiral or vortex solutions. As we shall discuss, there are, however, also some differences between these cases.

We will briefly indicate how the threshold between absolute and convective instabilities is calculated (see also [104]). The advection of a small perturbation is given by the nonlinear group velocity $s = \partial\omega/\partial q$ which is the sum of the linear group velocity s_0 and the nonlinear term $s_q := 2q(c_1 + c_3)$:

$$s_{\mathrm{L}} = -s_0 + 2q_{\mathrm{L}}(c_1 + c_3), \quad s_{\mathrm{R}} = s_0 + 2q_{\mathrm{R}}(c_1 + c_3). \tag{31}$$

The spreading velocity of perturbations is conveniently calculated in the linear marginal stability/pulled front framework [81–84,88,89] once one has obtained a dispersion relation for these perturbations. Since we consider single mode patches, we are allowed to restrict ourselves to a single CGL equation, in which the linear group velocity term $\pm s_0\partial_x A$ is easily incorporated, as it just gives a constant boost. Considering a perturbed plane wave of the form $A = (a + u)\exp \mathrm{i}(qx - \omega t)$, where u is a small complex-valued perturbation $\sim \exp \mathrm{i}(kx - \sigma t)$ and $a^2 = \varepsilon - q^2$. Upon substituting this Ansatz into a single CGL equation, linearizing and going to a Fourier representation, one obtains a dispersion relation $\sigma(k)$ [105]. From this relation one then finally calculates the spreading velocity v^*_{BF} of the Benjamin–Feir perturbations in the linear marginal stability or saddle-point framework [81–84].

Since in general we can only calculate the selected wavenumber q by a shooting procedure of the ODE's (12)–(15) for a source, obtaining a full overview of the stability of the plane waves as a function of the coefficients necessarily involves extensive numerical calculations. Therefore, we will focus now on a single sweep of c_2. For reasons to be made clear below, we choose $\varepsilon = 1$, $c_1 = c_3 = 0.9$, $s_0 = 0.1$ and $g_2 = 2$. Since we fix all coefficients but c_2, the stability boundary Eq. (30) is fixed. By sweeping c_2, the selected wavenumber varies over a range of order 1, and one encounters both convective and absolute instabilities.

[10] It should be noted that the criterion for absolute instability concerns the propagation of perturbations in an ideal, homogeneous background. For typical source/sink patterns, one has finite patches; the criterion can also not determine when perturbations are strong enough to really affect the core of the sources. Analogous to the 2D case, we have found that persistent dynamics sets in slightly *above* the threshold between convective and absolute instabilities.

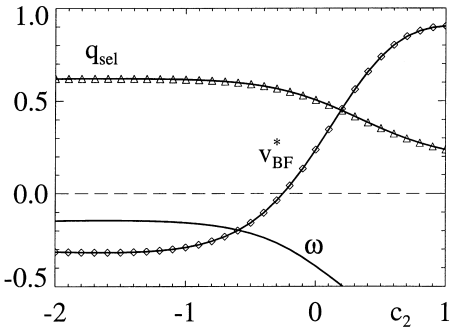

Fig. 6. Frequency ω, corresponding selected wavenumber $q_{\rm sel}$ and perturbation velocity $v^*_{\rm BF}$ as a function of c_2, for $\varepsilon = 1$, $c_1 = c_3 = 0.9$, $s_0 = 0.1$ and $g_2 = 2$. For $c_2 < -0.25$, $v^*_{\rm BF} < 0$, and perturbations in the right-flank of the source propagate to the left, so that the waves are absolutely unstable.

We have found that after a transient, patterns in the stable or convectively unstable case are indistinguishable [11]. When there is no inherent source of noise or perturbations, there is nothing that can be amplified, and the convective instability is rendered powerless (see however, Section 5.3).

Although the transition between stable and convectively unstable waves is not very relevant for the source/sinks patterns here, the transition between convectively and absolutely unstable waves is interesting. To obtain an absolute instability one needs to carefully choose the parameters; when q increases, the contribution to the group velocity of the nonlinear term s_q increases, and we have to take c_1 and c_3 quite close to the $c_1c_3 = 1$ curve to find absolute instabilities. This is the reason for our choice of coefficients. In Fig. 6 we have plotted the selected frequency (obtained by shooting), corresponding wavenumber and propagation velocity $v^*_{\rm BF}$ of the mode to the right of the source, as a function of c_2. For this choice of coefficients the single mode waves turn Benjamin–Feir convectively unstable when, accordingly to Eq. (30) $|q| > 0.223$, which is the case for all values of c_2 shown in Fig. 6. The waves turn absolutely unstable when $|q| > 0.553$, and this yields that the waves become absolutely unstable for $c_2 < -0.25$.

When the selected waves becomes absolutely unstable, the sources may be destroyed since perturbations can no longer be advected away from them; the system typically ends up in a chaotic state. In Fig. 7 we show what happens when we choose the coefficients as in Fig. 6, and decrease c_2 deeper and deeper into the absolutely unstable regime. All runs start from random initial conditions, and a transient of $t = 10^4$ was deleted. Although the left- and right traveling waves do not totally suppress each other, it was found that pictures of $|A_{\rm L}|$ and $|A_{\rm R}|$ are, to within good approximation, each others negative (see also the final states in Fig. 8). In accordance with this, we choose our greyscale coding to correspond to $|A_{\rm R}|$, such that light areas correspond to right-traveling waves and dark ones to left-traveling waves.

In Fig. 7(a), $c_2 = -0.3$ and the waves have just turned absolutely unstable, but the only nontrivial dynamics is a very slow drift of some of the sources and sinks. Note that this does not invalidate our counting results that isolated sources are typically stationary, because the drifting occurs only for structures that are close together. When c_2 is lowered to -0.4 (Fig. 7(b)), one can see now the Benjamin–Feir perturbations spreading out in the opposite direction of the group velocity, eventually affecting the sources (for example around $x = 230$, $t = 2700$). Some of the sinks become very irregular. When c_2 is decreased even further to -0.6 (Fig. 7(c)), the sources and sinks show a tendency to form periodic states [57,58] (see also Fig. 8). These states seem at most weakly unstable since only some very mild oscillations are observed. The two sinks with the largest patches around them show most dynamics, and one sees the irregular creation and annihilation of small source/sink pairs here (around $x = 320$ and 440). Finally,

[11] Except, of course, when we prepare a very large system with widely separated sources and sinks.

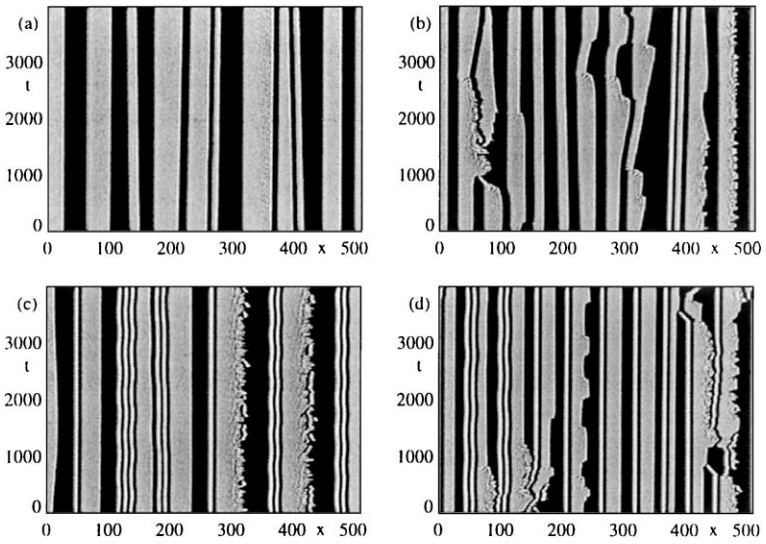

Fig. 7. Source/sink patterns with absolutely unstable selected wavenumbers for the same coefficients as in Fig. 6 and various values of c_2. (a) $c_2 = -0.3$, (b) $c_2 = -0.4$, (c) $c_2 = -0.6$, (d) $c_2 = -0.8$. For more information see text.

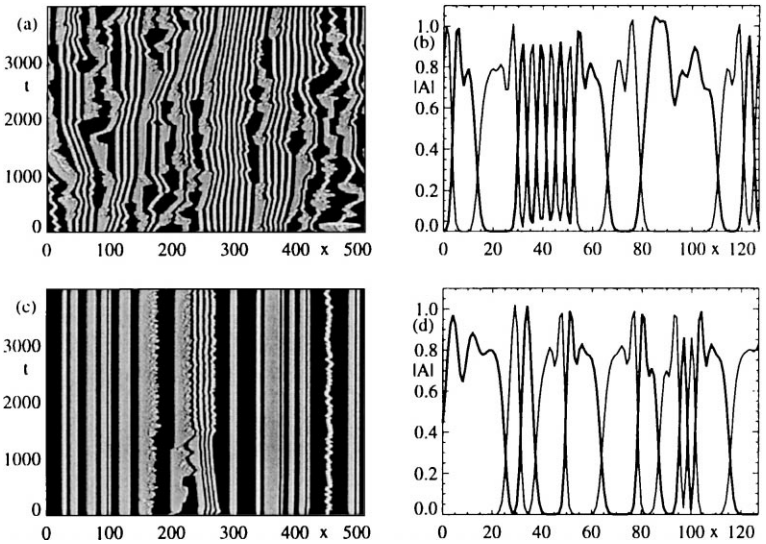

Fig. 8. Two more examples of nontrivial dynamics in the absolutely unstable case. Both cases: $c_1 = c_3 = 0.9$, $c_2 = -2.6$, $g_2 = 2$, and a transient of 10^4 is deleted. (a-b): $s_0 = 0.1$. Here the periodic states are quite dominant. It appears that these states themselves are prone to drifting and slow dynamics. (b) Snapshots of $|A_L|$ (thick curve) and $|A_R|$ (thin curve) in the final state. Obviously, the two modes, although disordered, suppress each other completely. (c–d) Here we have increased s_0 to 0.2. The plane waves are still absolutely unstable, and the dynamics is disordered, but much less than in case (a–b).

when c_2 is decreased to -0.8 (Fig. 7(d)) the state becomes more and more disordered; the irregular "jumping" sink at $x \approx 230$ is worth noting here.

It is interesting to note that, in particular for large negative c_2 closely bound, uniformly drifting sink-source pairs are formed (see for instance around $x = 430$, $t = 700$ in Fig. 7(d)). Another frequently occurring type of solution are periodic states, corresponding to an array of alternating patches of A_L and A_R mode (see also Fig. 8). The

source/sink pairs and in particular the periodic states occur over a quite wide range of coefficients; their existence has been reported before by Sakaguchi [57,58]. In a coherent structures framework, periodic states correspond to limit cycles of the ODE's (12)–(15). In many cases they can be seen as strongly nonlinear standing waves, and they show an interesting destabilization route to chaos (see Section 5.3.4).

Apart from the similarities between the mechanisms here and the spiral chaos of the 2D CGL equation, it is also enlightening to notice the differences. The first difference is that our sources, in contrast to the spirals in 2D, are not topologically stable. In the states we have shown so far this does not play a role; in the following section we will see examples where instabilities of the sources themselves play a role. While in the 2D case the spiral cores that play the role of a source are created and annihilated in pairs, it is here only the sources and sinks that are created or annihilated in pairs. Furthermore, in the spiral case, the linear analysis that determines whether the waves are absolutely of convectively unstable is performed for plane waves. This means one neglects curvature corrections of the order $1/r$, where r is the distance to the core of the source. Here, the only correction comes from the asymptotic, exponential approach of the wave to a plane wave; this exponential decay rate is given by the decay rate κ (see the Appendix). Finally, in the spiral case, for fixed c_1 and c_3, both the group velocity and the selected wavenumber are fixed, while here the selected wavenumber can be tuned by c_2, without influencing the stability boundaries of the single mode state. The group velocity can be tuned by s_0. Although the selected wavenumber influences the group velocity, cf. Eq. (31), and s_0 influences the selected wavenumber, this large number of coefficients gives us more freedom to tune the instabilities.

5.2. Instability to bimodal states: source-induced bimodal chaos

The dynamics we study in this section is intrinsically due to a competition between the single source-selected waves and bimodal states. Therefore, this state is in an essential way different from what can be found in a single CGL equation framework.

The wavenumber selection by the sources is of importance to understand the competition between single mode and bimodal states. In the usual stability analysis of the single mode and bimodal states, it is assumed that both the A_{L} and A_{R} modes have equal wavenumber [56]. Therefore, this analysis does not apply to the case of a single mode, say the right-traveling mode, with nonzero wavenumber. The left-traveling mode is then in the zero amplitude state and has no well-defined wavenumber; one should consider therefore its fastest growing mode, i.e., a wavenumber of zero. The following, limited analysis, already shows that for g_2 just above 1, instabilities are expected to occur. Restricting ourselves to long wavelength instabilities, the analysis is simply as follows. Write the left- and right-traveling waves as the product of a time dependent amplitude and a plane wave solution:

$$A_{\mathrm{L}} = a_{\mathrm{L}}(t)\mathrm{e}^{\mathrm{i}(q_{\mathrm{L}}x-\omega_{\mathrm{L}}t)}, \quad A_{\mathrm{R}} = a_{\mathrm{R}}(t)\mathrm{e}^{\mathrm{i}(q_{\mathrm{R}}x-\omega_{\mathrm{R}}t)}, \tag{32}$$

and substitute this Ansatz in the coupled CGL equations. One obtains then the following set of ODE's

$$\partial_t a_{\mathrm{L}} = (\varepsilon - q_{\mathrm{L}}^2 - a_{\mathrm{L}}^2 - g_2 a_{\mathrm{R}}^2)a_{\mathrm{L}}, \quad \partial_t a_{\mathrm{R}} = (\varepsilon - q_{\mathrm{R}}^2 - a_{\mathrm{R}}^2 - g_2 a_{\mathrm{L}}^2)a_{\mathrm{R}}. \tag{33}$$

Consider the single mode state with $a_{\mathrm{R}} \neq 0$, $a_{\mathrm{L}} = 0$ and take $q_{\mathrm{L}} = 0$. The maximum linear growth rate of a_{L} now follows from Eq. (33) to be the one with $q_{\mathrm{L}} = 0$; this mode has a growth rate given by $\varepsilon - g_2 a_{\mathrm{R}}^2 = \varepsilon - g_2(\varepsilon - q_{\mathrm{R}}^2)$. From this it follows that a single mode state with wavenumber q_{R} is unstable when $g_2 < \varepsilon/(\varepsilon - q_{\mathrm{R}}^2)$. In source/sink patterns, the selected wavenumber is as large as $\sqrt{\varepsilon/3}$ at the edge of the stability band for $c_1 = c_3 = 0$; it is as large as $0.6\sqrt{\varepsilon}$ in Fig. 6. In extreme cases, the value of g_2 necessary to stabilize plane waves can be at least 50% larger than the value 1 that one would expect naively.

On the other hand, the stability analysis of the bimodal states shows that they are certainly unstable for $g_2 > 1$. A naïve analysis for general q_{L} and q_{R}, based on Eq. (33) can be performed as follows. Solving the fixed point

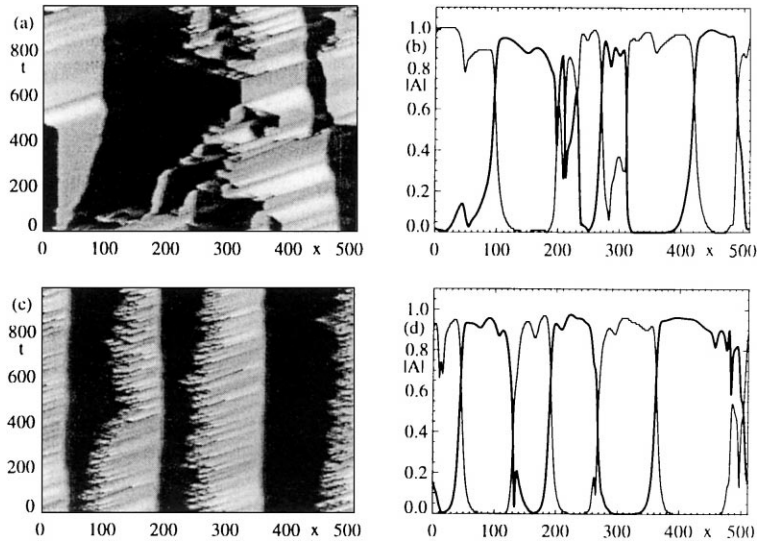

Fig. 9. Two examples of bimodal chaos. (a) and (c) show space time plots, and the grey shading is the same as before. Both simulations started from random initial conditions, and a transient of $t = 10^4$ has been deleted from these pictures. For a detailed description, see text. Note that the final states of runs (a) and (c), depicted in (b) and (d), clearly show that the two modes no longer suppress each other completely.

equations of Eq. (33) for the bimodal state (i.e., a_L and a_R both unequal to zero), and linearizing around this fixed point yields a 2×2 matrix. From an inspection of the eigenvalues we find that the bimodal states turn unstable when $g_2 < \varepsilon - q_1^2/(\varepsilon - q_2^2)$, where q_1 is the largest and q_2 is the smallest of the wavenumbers q_L, q_R. When both wavenumbers are equal this critical value of g_2 is one; it is smaller in general.

It should be noted that this analysis does not capture sideband instabilities that may occur, and therefore waves in a much wider range might be unstable. For sideband-instabilities of bimodal states, the reader may consult [56] and [106]. However, our analysis shows already that there is certainly a regime around $g_2 = 1$ where *both* the single and bimodal states are unstable. This regime at least includes the range $1 < g_2 < \varepsilon/(\varepsilon - q_{sel}^2)$.

The distinction between convective and absolute instabilities becomes slightly blurred here. Suppose for instance we inspect a single-mode state that turns unstable against bimodal perturbations. Initially, these perturbations will be advected by the group velocity of the nonlinear mode, but as the perturbations grow, both modes will start to play a role, and since they feel a group velocity of opposite sign, the perturbations are effectively slowed down. Roughly speaking, the instability might be linearly convectively unstable but nonlinearly absolutely unstable [99,100].

Without going into further details we will now show two examples of the bimodal chaos that occurs when g_2 is just above 1. For examples of similar dynamics, also for $g_2 < 1$, see [106]. In the first example (Fig. 9(a) and (b)) we have taken $\varepsilon = 1, c_1 = c_3 = 0.5, c_2 = -0.7, s_0 = 1$ and $g_2 = 1.1$. The selected wavenumber is almost independent of the value of g_2 and approximately equal to 0.35, which yields a critical value of g_2 of 1.14. For g_2 just below this value, the instability appears convective, and after a transient the system ends up in a mildly fluctuating source/sink pattern. When g_2 is decreased, the instability becomes stronger and, presumably, absolute in nature. The *sources* behave then very irregularly, while the sinks drift according to there incoming, disordered waves. Note that sources and sinks are created and annihilated in this state. In Fig. 9(c) and (d) we show the disordered dynamics for $\varepsilon = 1, c_1 = 1, c_3 = -1, c_2 = 1, s_0 = 0.5$ and $g_2 = 1.1$. Note that in the laminar patches, since $c_1 = -c_3$, the dynamics is relaxational [2,4]. In this state, no creation or annihilation of sources and sinks is found; the sinks drift slowly, while the sources behave very irregularly.

The dynamical states as shown in Fig. 9 are different from the chaotic states that we are familiar with from the single CGL equation [63–65,67], and so they are of some interest in their own right. Note that it is possible to get persistent dynamics for values of c_1 and c_3 that in a single CGL equation-framework would lead to completely orderly dynamics. As the two examples in Fig. 9 show, qualitatively different states seem to be possible in this regime; the question of classification of the various dynamical states is completely open as far as we are aware.

Finally, it should be pointed out that when, as is the case here, the left-and right-traveling mode no longer suppress each other, $\varepsilon_{\mathrm{eff}}$ becomes positive. In principle this might change the multiplicity of the sources, since the eigenvalues coming from the linear fixed point can have a different structure for positive $\varepsilon_{\mathrm{eff}}$ (see Section B.7). However, this is only true when the effective velocity $v \pm s_0$ is larger than the critical velocity v_{cL}; for the cases considered above, this does not happen. Hence, the sources are here still unique and select a unique wavenumber.

5.3. Mixed mechanisms

In the previous sections we have described three mechanisms by which sink-source patterns can be destabilized. First of all, in Section 4 we found that due to a competition between the linear group velocity s_0 and the propagation of linear fronts, the cores of the sources become unstable when $\varepsilon < \varepsilon_{\mathrm{c}}^{\mathrm{so}}$. In Section 5.1 we have shown that the waves that are sent out by the sources can be convectively or even absolutely unstable, and in Section 5.2 we found that these waves may also be unstable to bimodal perturbations when g_2 is not very far above 1. Since the mechanisms that lead to these instabilities are independent, these instabilities might occur together. This is the subject of this section. In particular, one can always lower the control parameter ε in an experiment to make the sources become core-unstable (Section 5.3.1). A second combination of instabilities occurs when g_2 is close to 1 and the plane waves are unstable and generate phase slips (Section 5.3.2); a particular interesting case occurs when the single mode waves are in the so-called intermittent regime (Section 5.3.3).

5.3.1. Core instabilities and unstable waves

As discussed in Section 4.2, the cores of the source may start to fluctuate when $\varepsilon < \varepsilon_{\mathrm{c}}^{\mathrm{so}}$. As is visible in Fig. 4(c), the perturbations that are generated in the core are then advected away into the asymptotic plane waves. In the discussions in Section 4, we have focused on the case where these waves are stable, but obviously, when they are unstable, this will amplify the perturbations emitted by the source core. In particular, when the waves are convectively unstable, a stable core for $\varepsilon > \varepsilon_{\mathrm{c}}^{\mathrm{so}}$ leads to stationary patterns, but a fluctuating core can fuel the convective instabilities. This yields a simple experimental protocol to check for convective instabilities; simply lower ε and follow the perturbations send by the sources for $\varepsilon > \varepsilon_{\mathrm{c}}^{\mathrm{so}}$.

5.3.2. Phase slips and bimodal instabilities

Let us for definiteness suppose we have that $A_{\mathrm{L}} = 0$, and the right-traveling mode is active. When this A_{R} mode is chaotic and displays phase slips, the effective growth rate of the A_{L} mode, $\varepsilon_{\mathrm{eff}}^{\mathrm{L}}$, may become positive for some period. A_{L} only grows during this period; it depends then on the duration and spatial extension of the positive $\varepsilon_{\mathrm{eff}}^{\mathrm{L}}$ "pocket" whether A_{L} can grow on average. Clearly, one should look at a properly averaged value of $\varepsilon_{\mathrm{eff}}^{\mathrm{L}}$, and therefore at the averages of $\varepsilon - g_2 a_{\mathrm{R}}^2$ [57,58]. When g_2 is sufficiently large, the averaged effective growth rate always becomes negative, so that even a heavily phase slipping wave can still suppress its counter-propagating partner.

We show two examples of the dynamics when phase slips occur and g_2 is not large enough to strictly suppress the near-zero mode. As coefficients we choose $c_1 = 1, c_3 = 1.4, c_2 = 1, \varepsilon = 1, s_0 = 0.5$, and the dynamics is illustrated in Fig. 10. It should be noted that in Fig. 10(b) the sources are stationary, while some of the sinks drift. This seems to be due to the fact that near the sink, i.e., far away from the sources, the wave emitted by the sources has undergone phase slips, and the incoming wavenumbers of the sink can therefore be different from the

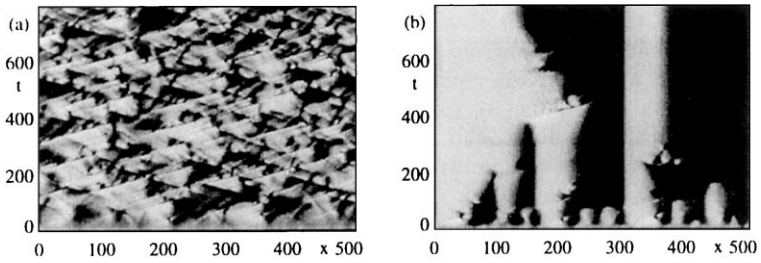

Fig. 10. Two examples of the combination of phase slips and a value of g_2 just above 1. The coefficients are $c_1 = 1, c_3 = 1.4$, $c_2 = 1, \varepsilon = 1, s_0 = 0.5$. Grey shading as before (right (left) traveling waves are light (dark)). In (a), $g_2 = 1.05$, while in (b) $g_2 = 1.2$.

source-selected wavenumbers. For slightly different coefficients we have observed patterns of stationary sources, with sinks in between that by this mechanism move in zig-zag fashion, i.e., alternating to the left and to the right.

5.3.3. Intermittency and bimodal instabilities

Recently, Amengual et al. studied the case of spatio-temporal intermittency in the coupled CGL equations for a linear group velocity $s_0 = 0$ and $c_2 = c_3$ [59]. This particular sub-case of the coupled CGL equations is of importance in the description of some laser systems [59–61]. When g_2 is increased from zero, the authors of [59] found that for $g_2 < 1$ one finds intermittency, with the A_L and A_R obviously becoming more and more correlated as the cross-coupling increases. Furthermore, the authors observed that for $g_2 > 1$, the two modes become "synchronized", i.e., the intermittency disappears and the systems ends up in a state that we recognize now as a stationary source/source pattern (not source/sink). Since the intermittency "disappears" the authors question the applicability of a single CGL equation for patches of single modes in the coupled CGL equations (2) and (3).

The purpose of this section is to clarify, correct and extend their results, using our results for the wavenumber selection, the bimodal instabilities and the discussion in Section 5.3.2. In particular we will show that, (i) for sufficiently large g_2, the intermittency can persist, (ii) when the intermittency disappears it can do so by at least two distinct mechanisms, (iii) more complicated states can occur. We conclude then that for single mode patches the single CGL is a correct description, provided one is sufficiently far away from bimodal instabilities and one takes the source-selected wavenumber and correct boundary conditions into account.

For the case considered in [59] the group-velocity s_0 is equal to zero, so the two modes A_L and A_R are completely equivalent. The distinction between sources and sinks depends therefore on the nonlinear group velocity, which follows from the selected wavenumber. The counting arguments yield in this case again a discrete $v = 0$ source and a two-parameter family of sinks (see Section 3). In simulations we typically find stationary sources that separate the patches of A_L and A_R mode, and *single amplitude sinks* sandwiched in between these sources.

We will show now a variety of scenarios for intermittency in the coupled CGL equations (2) and (3). The coefficients used in [59] are $c_1 = 0.2, c_2 = c_3 = 2, \varepsilon = 1$ and $s_0 = 0$. The coefficients c_1 and c_3 are chosen such that a single mode is in the so-called intermittent regime. In this regime, depending on initial conditions, one may either obtain a plane wave attractor or a chaotic, "intermittent" state; the latter one is typically built up from propagating homoclinic holes and phase slips [63–65,67].

In Fig. 11(a) we take $g_2 = 2$ and start from an ordered pair of sources. By a rapidly changing c_1 to a value of 1.2 and then back to the value 0.2, we generate phase slips that nucleate a typical intermittent state. This intermittent state persists for long times; there is no "synchronization" whatsoever. We found that we can also first let the source develop completely, and then introduce some phase slips; also in this case the intermittency clearly persists. To understand this, note that in this case g_2 is sufficiently large, and so ε_{eff} is negative (see Section 5.3.2); although there are phase slips, the two modes suppress each other completely.

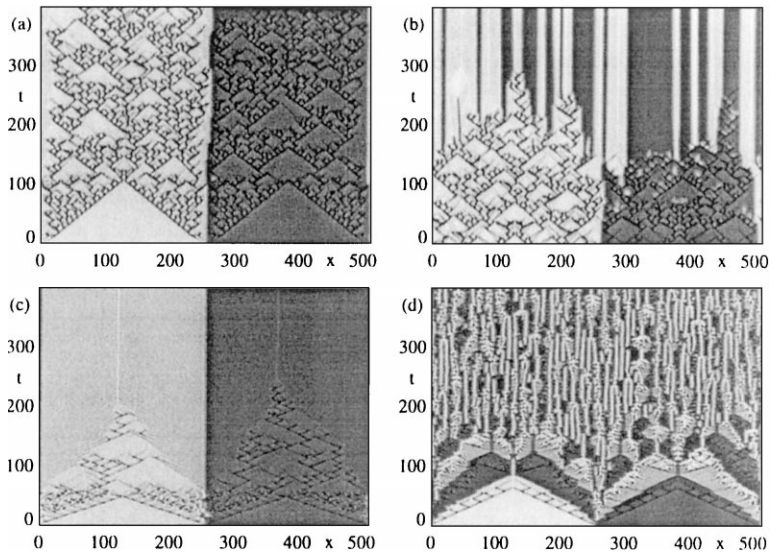

Fig. 11. Space–time plots in the coupled-intermittent regime. To be able to show both the dynamics in the A_L and A_R mode, the grey shading corresponds to $2|A_R| + |A_L|$. This yields that right traveling patches are brighter in shade than left-traveling patches. (a) $c_1 = 0.2, c_2 = c_3 = 2, \varepsilon = 1, s_0 = 0$ and $g_2 = 1.2$. (b) Same coefficients as (a), except for $g_2 = 1.5$. (c) $c_1 = 0.6, c_3 = 1.4$, $c_2 = 1, \varepsilon = 1, s_0 = 0.1$ and $g_2 = 2$. (d) Same coefficients as (c), except for $c_2 = 0$. For as more detailed description see text.

In contrast, when g_2 is lowered, ε_{eff} can become positive, and this corresponds to the scenario described in [59]. In Fig. 11(b) we start from state obtained for g_2=2, and then quench g_2 to a value of 1.5. In this case, ε_{eff} becomes positive every now and then, and after a while, in the patch originally the exclusive domain of A_L, small blobs of A_R mode grow. After a sufficient period has elapsed, these blobs nucleate new sources, and the system ends up in a stationary source/source pattern. The laminar patches in between the sources are quite small and the intermittency disappears.

The system switches from the intermittent to the plane wave attractor when the new sources are formed; this does not mean that the CGL equation is incorrect here, since both plane waves and intermittent states are attractors for these coefficients. The disappearance of the intermittency can be easily understood as follows: the main mechanism by which intermittency spreads through the single CGL equation is by the propagation of homoclinic holes that are connected by phase slip events [67]. If the phase slips now generate sources, there is no generation of new homoclinic holes and the intermittency dies out.

It should be noted that for this particular choice of the coefficients c_1 and c_3, the homoclinic holes have a quite deep minimum in $|A|$, which increases the value of the average of ε_{eff}; therefore one needs quite a large g_2 to guarantee the mutual suppression of the A_L and A_R modes.

Finally, we found that the selected wavenumber for the coefficients of this particular example is ≈ 0.1. As a consequence, the transition to stationary domains as observed in [59] can *not* occur at g_2 precisely equal to 1, but occurs for $g_2 \approx 1.01$ (see Section 5.2).

This generation of sources due to phase slips of the nonlinear mode is not the only way in which the intermittency can disappear. Consider the example shown in Fig. 11(c). We have chosen the coefficients as $c_1 = 0.6, c_3 = 1.4, c_2 = 1, \varepsilon = 1, s_0 = 0.1$ and $g_2 = 2$. The sources select now a wavenumber of 0.3783, and the plane wave emitted by the source simply "eats up" the intermittent state; note the single amplitude sinks visible for late times. It should be realized that many dynamical states are sensitive to a background wavenumber, and that the spatio-temporal intermittent state is particularly sensitive to this [67]; when describing a patch in the coupled CGL

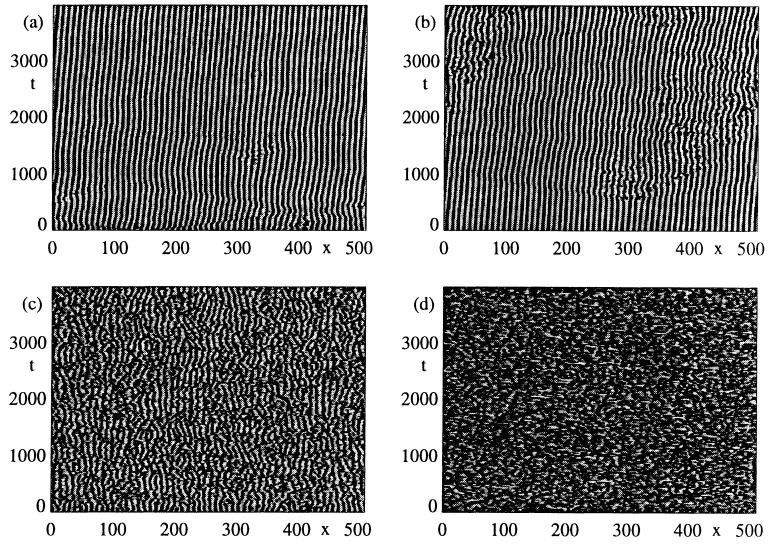

Fig. 12. Four space–time plots, showing the transition from standing waves to disordered patterns, for $g_2 = 1.1, c_1 = 0.9, c_3 = 2$, $s_0 = -0.1, \varepsilon = 1$, and (a) $c_2 = -0.72$, (b) $c_2 = -0.71$, (c) $c_2 = -0.5$, (d) $c_2 = 0$. See text.

equations by a single CGL equation, one should take into account that one has wave-selection at the boundaries due to the sources.

Finally, when c_2 is lowered to a value of 0, the sources themselves become unstable and the system displays the tendency to form periodic patterns; these are however not stable, and an example of the peculiar dynamical states one finds is shown in Fig. 11(d).

In conclusion, when one is far away from any bimodal instabilities, i.e., when g_2 is sufficiently large, a description in terms of a single CGL equation is sufficient for the patches separating the sources, provided one takes into account the group velocity, boundary effects and, most importantly, the selected wavenumber. It is amusing to note that the question under which conditions a single amplitude equation is a correct description of these waves depends on the coefficients g_2 and c_2 of the *cross-coupling* term.

5.3.4. Periodic and other states

We would like to conclude this section by showing an example of the wide range of different states that occur in the coupled amplitude equations when we sweep c_2. We choose the other coefficients as follows: $g_2 = 1.1, c_1 = 0.9, c_3 = 2, s_0 = -0.1, \varepsilon = 1$. Our main finding is that for large positive or negative c_2, their is no sustained dynamics, while for small c_2 we find a strongly chaotic state. In between there are at least two transitions between laminar and disordered state (see Figs. 12 and 13).

For sufficiently negative c_2, all initial conditions evolve to a spatially periodic state, with rapidly alternating A_{L} and A_{R} patches. We can view these states as an example of highly nonlinear standing wave patterns. Depending on initial conditions, these states may either be stationary or have a small drift. For our particular choice of coefficients it is empirically found that these states are linearly stable for $c_2 \leq -0.72$. In Fig. 12(a) we see the evolution from a slightly perturbed initial condition for this value of c_2. Qualitatively, we observe that when the "local wavenumber" of the standing wave is lowered, this leads to oscillations, that may or may not lead to "defects". After some reasonably long transient (note the perturbation at $x \approx 320, t \approx 2600$), the dynamics settles down in a slowly drifting standing wave. This shows that these generalized standing waves are stable here.

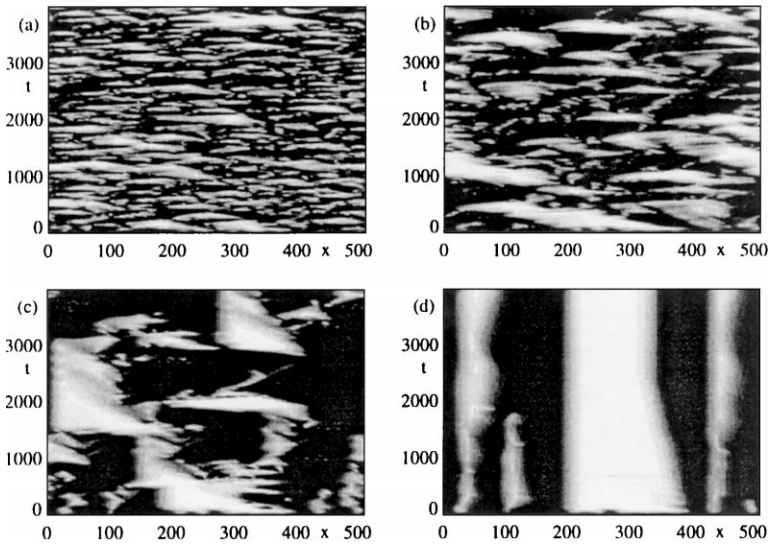

Fig. 13. Four space–time plots for the same coefficients as in Fig. 12, but now for positive values of c_2. (a) $c_2 = 0.8$, (b) $c_2 = 0.9$, (c) $c_2 = 0.95$, (d) $c_2 = 1$.

In Fig. 12(b) we start from such a coherent standing wave state and have lowered c_2 to a value of -0.71. In this case perturbations of the waves are spontaneously formed, indicating a linear instability. Since the state is unstable, these perturbations then spread to the system in a way that is reminiscent of the intermittent patterns obtained, for instance, in experiments on intermittency in Rayleigh–Bénard convection [107,108]. It should be noted that, due to the instability of the laminar state, one does not have an absorbing state, so strictly speaking this state should not be referred to as intermittent. Interestingly enough, the transition between laminar and chaotic behavior seems to be second order, i.e., we could not find any hysteresis. The transition is simply triggered by the linear stability of the periodic/standing waves, and when these waves are stable, they are the only type of attractor.

If c_2 is further increased to a value of -0.5 (Fig. 12(c)), we find a state that we might call defect-chaos of a standing wave pattern. For $c_2 = 0$ (Fig. 12(d)), the dynamics evolves on much faster time-scales, and no clear structures are visible by eye.

On the other hand, when we keep increasing c_2, we again find regular states, but these ones correspond to stationary source/sink patterns. This is illustrated in Fig. 13, where we show four space–time plots for increasing, positive values of c_2. In comparison with the dynamics as shown in Fig. 12(d), the time scales become slower and slower when c_2 is increased. This slowing down becomes quite clear for $c_2 = 0.8$ (Fig. 13(a)) and $c_2 = 0.9$ (Fig. 13(b)). For $c_2 = 0.95$ (Fig. 13(c)), the dynamics becomes even more slow and regular. We clearly see now stationary sources, with irregularly moving sinks in between. Due to the smallness of g_2, phase slips in one of the single modes leads in some case to the formation of new sources and sinks. When c_2 is increased to a value of 1 (Fig. 13(d)), some slow dynamics sets in, that may or may not be a long living transient. For values of c_2 above 1.1, all initial conditions seem to evolve to a stationary, regular source/sink pattern.

6. Outlook and open problems

In this paper we have extended the coherent structures framework and the counting arguments to the coupled CGL equations, and obtained important information on the dynamical states that are independent of the precise values

of the coefficients and bear experimental relevance. In general, these considerations lead to the conclusion that sources are often unique, sometimes come in pairs but in any case are at most members of a discrete set of solutions. As a result, they are instrumental for the wavenumber selection of both regular and chaotic patterns. Many of the instability mechanisms and dynamical regimes of the coupled CGL equations can be understood qualitatively from this point of view, and we have shown several examples of hitherto unexplored regimes of persistent spatio-temporal chaotic dynamics (see Table 1). In this closing section, we wish to discuss some of these findings in the light of experimental observations, and summarize the most important open theoretical problems.

6.1. Experimental implications

In short, the experimental predictions that we make, based on our study of the coupled CGL equations are the following:

- *Multiplicity.* Our analysis shows that sources are expected to come in a discrete set, which would experimentally amount to a *unique*, stationary source. Furthermore, this source is expected to be *symmetric*, in that it sends out waves of the same wavenumber to both sides.

  Sinks are non-unique. This means that one could have sinks with different velocities present at the same time. In light of the previous remark on the uniqueness of sources, this might prove hard to observe experimentally.
- *Wavenumber selection.* One important consequence of the uniqueness of sources is that they select an asymptotic wavenumber, just as spirals do in the 2D-case. Since the traveling-wave system is quasi-one-dimensional however, we expect the wavenumber selection to be much easier to study.
- *Scaling behavior.* We have made definite predictions for the small-ε scaling of the width of sources and sinks. Moreover, we predict the stationary sources to disappear at some finite value of ε, which is the point where the non-stationary sources take over. These sources scale as ε^{-1}, as do the sinks.
- *Instabilities and dynamical behavior.* Apart from the non-stationary sources that occur when ε is decreased sufficiently, we have found that there are at least two other mechanisms leading to dynamical states. The central observation is that the waves that are selected and sent out by the sources may become unstable. Similar to what happens in the single CGL equation, these waves can become convectively or absolutely unstable; the latter case in particular yields chaotic states (Section 5.1). When the cross-coupling coefficient is not too far above one, and the selected wavenumber is unequal to zero, there is a regime where both single and bimodal states are unstable.

6.2. Comparison of results with experimental data

Most research in the field of traveling wave systems has focussed on the properties of the single-mode states, i.e., the states where the entire experimental cell is filled up by either the left-or the right-traveling wave. From such a perspective, it is natural to disregard the source/sink patterns that generally occur initially above onset as unwanted transient states. Consequently they have not been studied as extensively as we think they deserve to be. It is the aim of this section to confront a number of the theoretical findings of this article with some of the experimental observations in the heated wire experiments [33–36] and in the experiments on traveling waves in binary liquids [37–39,109–111]. In no way do we claim this comparison to be exhaustive – the main aim of our discussion is to show that our results put various earlier observations in a new light, and that it should be feasible to settle various of the issues we raise with further systematic experiments.

6.2.1. Heated wire experiments

When a wire which is put a distance of the order of a millimeter under the free surface of a liquid layer is heated, traveling waves occur beyond some critical value of the heating power [33–36]. This bifurcation towards traveling

waves turns out to be supercritical [36], and the group velocity and phase velocity turn out to have the same sign in the experiments [33] [12]. The paper by Vince and Dubois [36] is one of the few papers we know of that discusses the ε-dependence of the width of sources. The authors show that the inverse width scales linearly with the heating power Q, and associate this with a scaling of the source width as ε^{-1}. This is correct if the value of Q at which the source width diverges coincides with the threshold value for the linear instability, but whether this is actually the case is unfortunately not quite clear from the published data [13]. Formulated differently, in terms of our numerical data shown in Fig. 4(d), the question arises whether in the experiments the approximate linear scaling of the inverse width with the heating power was associated with that of the thick line above ε_c^{so}, or with the linear scaling $\sim \varepsilon$ below ε_c^{so}. If indeed the experiments are consistent with an ε^{-1} scaling of the width, then according to our analysis the sources should be (weakly) non-stationary and prone to pinning to inhomogeneities in the cell. If the source width diverges at a finite value of ε, this might be evidence for the existence of the critical value ε_c^{so}. It should be of interest to investigate this further.

In [34], Dubois et al. also note that "... *sources may be large when the sinks are always very narrow* ..." in their heated wire experiments. This agrees with our finding that sinks are always less wide than the sources but the published data do not allow us to extract the scaling of the sink width with ε.

In the experiments by Alvarez et al. [33], sources were found to be stationary and symmetric but non-unique, i.e., each source sends out the same waves to both sides, but different sources send out different waves. As a result, patches with different wavenumbers were found to be present in the system (at any one time), and the sources were seen to move in response to the fact that they were sandwiched between waves of different frequency. We have already seen in Section 3.3 that there are certain regions of parameter space where there were two different sources present at the same time (for one of them, the linear group velocity s_0 and nonlinear group velocity s had opposite signs). However, the fact that we can have various discrete source solutions can not explain the experimental observations. First of all, in our simulations two of such sources were separated by a sink-type structure in one single mode patch, *not* by a sink separating two oppositely traveling waves, as in the experiments. Secondly, in the experiments there were always slight differences between any two pair of sources, which appears inconsistent with the existence of a finite number of discrete source solutions.

It appears likely to us that the occurrence of slight differences between different sources results from the fact that there are always some impurities or inhomogeneities present in any experimental setup. Very much like the spirals and target patterns one encounters in the 2D CGL equation [112], coherent structures might well be pinned to such imperfections [14]. This would of course not invalidate the results of the counting arguments for the homogeneous case, as it is precisely on the basis of this counting argument that one would expect the properties of the discrete source solution(s) to depend sensitively on the local parameter values.

The sinks which in the experiments of [33] were sandwiched between two patches with different wavenumbers, were found to move according to what was referred to as a "phase matching rule": during the motion, a constant phase difference is maintained across the sink profile, so that no phase slip events occur. This commonly occurs for sinks in the *single* CGL equation, and Fig. 3 provides an example of this, but there is one important difference here: sinks in the experiments separate two oppositely traveling waves, so phase matching in the actual experiments involves the *fast* scales represented by the critical wavelength q_c of the pattern at onset. In the amplitude approach all information about this q_c is lost since we eliminated the fast scales and only consider the difference between the actual wavenumber q of the pattern and this q_c. At least in the experiments of [33] the coupling between the

[12] Fig. 11 of [36] also illustrates quite nicely that the group velocity and phase velocity are parallel.

[13] In the experiments shown in Fig. 10 of [36], the source width diverged at $Q \approx 4.2$ W. Unfortunately, the distance h between the wire and the fluid surface is not given for the data shown. All other measurements in the paper are made at $h = 1.34$ mm and $h = 1.97$ mm, and these values correspond to $Q_c \approx 2.5$ W and $Q_c \approx 2$ W.

[14] An example of how sources can be pinned near cell boundaries below ε_c^{so} is discussed in [52].

fast and the slow scales is important. These so-called *non-adiabatic* effects [98] will be the object of further study. Experimentally, it is not clear whether the "phase matching rule" was a peculiarity of [33], or whether it holds quite generally.

As we have seen in this paper, the wavenumber selection by sources entails various scenarios for instabilities and chaotic dynamics in the single-mode patches that are separated by sources and sinks. In the experiments, there are regimes in parameter space where the dynamics is reminiscent of what one expects when the mode selected by the sources becomes convectively or absolutely unstable. Whether the data are consistent with this scenario has remained unexplored, however.

We finally note that it has recently become apparent that traveling waves in convection cells with a free surface which are heated from the side [113–115], are intimately related to those occurring in the heated wire experiments [40]. Sources and sinks have also been observed in such experiments, but a systematic study of some of the issues we raise does not appear to have been undertaken yet. Clearly, both the heated wire experiments and this system appear to be very suitable setups to study the dynamics of sources and sinks; in addition, both do show rich dynamical behavior.

6.2.2. Binary mixtures

One of the best studied experimental traveling wave systems is binary fluid convection [37–39,110,111]. Since the bifurcation in this case has been shown to be weakly subcritical [21], the description of the behavior in this system is strictly speaking beyond the scope of the coupled CGL equations we consider. A brief discussion is nevertheless warranted, not only because some of the behavior of sources and sinks is quite generic, in that it does not strongly depend on the underlying bifurcation structure (e.g., sources still form a discrete set according to the counting arguments), but also because the additional complications of the binary mixture convection experiments are an interesting subject for future study.

Kaplan and Steinberg have shown that the transition from localized traveling wave patterns (pulses) to extended traveling waves is essentially governed by the convective instability of the edges of the pulses [41] [15] . The fact that the relevant front velocity is given by linear marginal stability arguments, suggests that the subcritical character of the bifurcation is not very strong here. On the other hand, the nonadiabatic effects, such as locking, observed in [42], point in the other direction, namely that the subcritical nature of the transition is rather strong. Hence, the importance of the subcritical effects in these experiments can not be trivially established.

Kolodner [38] has observed a wide variety of source/sink behavior. In some cases, there appears to be a stable source/sink pair where the sink is clearly wider than the source. This of course contradicts what we typically find (except close to the relaxational limit – see Section 4.4). This may have to do with the subcritical nature of the bifurcation, but one should also keep in mind that in other cases there is evidence that such behavior could still be a transient, because there are still phase slip events occurring. E.g., Fig. 5 of [38] shows a notable example of a case in which the sink is initially wider than the source, but in which a process clearly involving the fast scales narrows it down, so that in the end it smaller than the source.

Another interesting state that is encountered in the experiments are drifting source/sink patterns (see, e.g., Fig. 7 of [38]). The sources here move slowly but with a constant velocity, and are non-symmetric in that the wavenumbers on either side are different. However, there is again a one-to-one correspondence between the drift velocity and the difference in wavenumbers. In [38], this is referred to this process as "Doppler shifting", to indicate that in the frame co-moving with it, the drifting source sends out waves with the same frequency to the left and the right. This is completely equivalent to the "phase matching rule" of [33]. When such a moving source is present, the sinks are also found to obey the phase matching rule and so they move with exactly the same drift

[15] This is similar to the behavior of sources near ε_c^{so} (Section 1.2.2).

velocity as the sources. Clearly, it is still the source that selects the wave number and hence plays the active role here – as usual, the sink motion is essentially determined by the properties of the waves that come in. A priori, one could imagine that the sources and sinks in the binary fluid experiments are more prone towards obeying the phase matching rule due to the subcritical nature of the bifurcations to traveling waves, but one can find various examples in the experiments where they do not obey this rule. Obviously, this question deserves further study.

The fact that Kolodner [38] observes in his Fig. 7 a steadily moving source is not necessarily in contradiction with our counting arguments, as these do allow for the existence of a discrete set of $v \neq 0$ sources. In practice, however, for a proper analysis of such source solutions in the binary fluid experiments it is probably necessary to include the coupling to the slow concentration field, as in the work of Riecke et al. on traveling pulse solutions [16, 116,117].

Although several of the experiments of Kolodner have been done at very small values of ε, there is no visible evidence of the divergence of the width of any of the sources and sinks. Presumably, this is due to the subcritical nature of the bifurcation – in Section 4.2 we already argued that in this case the width of neither the sources nor the sinks need to diverge as $\varepsilon \to 0$.

In passing, we note that, quite impressively, Kolodner has also been able to extract the spatial amplitude profiles of his sources and sinks (Figs. 8, 18, 21 of [38]). These agree remarkably well with the profiles we obtained numerically using the shooting method described earlier. Even the characteristic overshoots of the amplitudes near the edges of sinks are clearly observable in all cases.

In conclusion, although a detailed comparison between the sources and sinks in binary fluid experiments and those analyzed theoretically here, is not justified, many qualitative features (multiplicity, wavenumber selection, etc.) are quite similar. We expect that the ε dependence of the width of these structures is very different in the two cases, due to the subcritical nature of the bifurcation in binary mixtures and due to the coupling to the slow concentration field. The latter effect probably also plays an important role in the drift of the sources.

6.3. Open problems

In spite of the fact that we have been able to map out many of the various possible static and dynamical properties of sources and sinks, there remains a large number of theoretical issues and open problems which need to be studied in further detail. This section briefly lists the ones we consider most important.

- *Phase matching.* The absence of the coupling of the phases across a moving sink appears to be one of the main short comings of the coupled CGL equations.

  For the single mode CGL equation, the velocity of sinks is determined in terms of the two wavenumbers q_{N_1} and q_{N_2} of the incoming modes, without solving for the structure of the sinks: $v = (c_1 + c_3)(q_{N_1} + q_{N_2})$ [68,69]. This follows directly from the requirement that in the frame moving with the sink, the frequencies to the left and the right of the sink should be equal. Phase slips occur when these frequencies are unequal, and in that case the sink is not a "coherent structure" (i.e., it has a time-dependent spatial profile).

  For the sinks in the coupled CGL equations ((2.6) and (3)) that we have studied here, the velocity of a moving sink can not be simply given in terms of the wavenumbers of the incoming waves – the velocity is determined implicitly by the solution of the ODE's Eqs. (12)–(15). The frequencies to the left and to the right of sinks correspond to two different modes, and the coupling between these modes depends only on their amplitudes, not on their phase. Moreover, the phase matching as observed empirically in the experiments [33] clearly involves the fast scale that has been eliminated to obtain the amplitude equations; therefore, such rule can never be implemented in the standard coupled CGL equations (2) and (3) [33].

The phase matching as observed in the experiments is clearly a non-adiabatic effect as it involves both the fast and the slow scales. Can this non-adiabatic effect be studied perturbatively, as in [98]? As pointed out to us by Newell, the experimental phase matching appears to be the analogue in space–time of what happens at grain boundaries in the phase equations in the nonlinear regime [3]. Does this analogy open up a route towards analyzing this effect?

- *Multiplicities.* In our counting analysis, we have focussed on the regime where $|v| < s_0$, and in particular on the case $v = 0$. From the results detailed in the appendix, it follows that the flow structure near the fixed points changes when $|v| > s_0$; this implies that the counting arguments allow for rapidly moving source and sinks solutions with different multiplicities. We do not know whether such solutions actually exist. We have not studied this possibility (nor the one associated with changes of the fixed point structure related to the critical velocity v_{cN}) in detail, as we have neither found such coherent structure solutions of the ODE's, nor observed any of them in numerical simulations of the coupled CGL equations.
- *Coherent structures.* When g_2 is large enough, single amplitude coherent structures such as sources, sinks and homoclinic holes are often exact solutions of the coupled CGL equations. One of the modes corresponds then to the coherent structure, the other mode is zero. To see this, note that solutions of the single CGL equation have often a minimum amplitude a_{m} which is nonzero. As long as $\varepsilon_{\mathrm{eff}} = \varepsilon - g_2 a_{\mathrm{m}}^2$ remains negative for the zero mode, this mode is suppressed. A detailed analysis of the behavior of such coherent structures as g_2 is reduced and the other mode becomes active, remains to be done.

  The closely bound source/sink pairs, as shown in Fig. 7(a) can be seen as a "new" coherent structure of the coupled CGL equations. We note that from a counting point of view, such source-sink pairs typically correspond to homoclinic orbits, since they often connect the same plane wave state to the left and the right. Irrespective of the details of the structure of the corresponding fixed point, one needs to satisfy in general one condition to obtain such a homoclinic orbit (One can see this easily as follows. Suppose the fixed point has a n-dimensional outgoing manifold. This yields $n - 1$ degrees of freedom and n conditions, so in general one parameter needs to be tuned to obtain a homoclinic orbit). Since we have three free parameters, this yields a two-parameter family of such sink-source pairs

  It would be interesting to investigate whether these homoclinic structures are connected to the homoclinic holes, analyzed recently for the single CGL equation [67]. It is conceivable that upon lowering g_2, the suppressed mode will mix in below some particular value of g_2, so that a homoclinic holes can be deformed to coupled sink-source pairs.

  A related issue is the study of the cross-over from an array of sources and sinks to an (almost) periodically modulated amplitude pattern of the type seen in Fig. 12 and by Sakaguchi [57,58].
- *Phase-space and dynamical arguments.* In Section 4.2, the existence of a special value $\varepsilon_{\mathrm{c}}^{\mathrm{so}}$ was obtained from what was essentially a dynamical argument. At this value of ε, the width of stationary sources, as determined by the set of ODE's Eqs. (12)–(15), was found to diverge. What is the precise connection between the phase-space structure of the ODE's and the dynamical argument? This question is related to that which arises in the study of nonlinear global modes, and it is quite possible that the analysis of [97] can be extended to sources as well.
- *Stability.* A full stability analysis of sources and sinks would be welcome, as most of our discussion on their stability is based on intuitive arguments. Such an analysis might well detect the existence of additional instability mechanisms associated with the existence of discrete core modes in much the same way as happened for pulses [90–92].
- *Breathing.* In Section 4.2, we noted that interactions between local structures and fronts often give rise to an oscillatory or "breathing" type of dynamics [94,95,116]. The mechanism through which this happens remain largely unexplored, however.

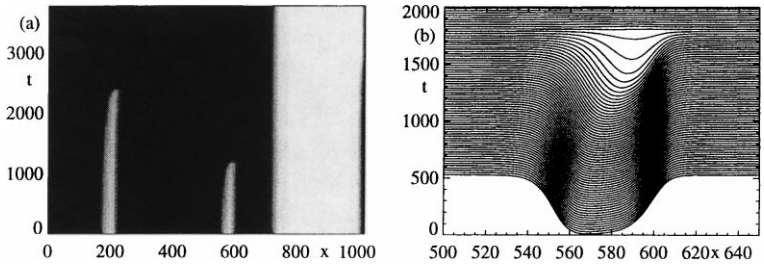

Fig. 14. (a) Space–time plot of $|A_R|$ illustrating the interaction between sources and sinks. The runs started from random initial conditions, and the coefficients were chosen as $c_1 = 0.6$, $c_3 = 0.4$, $c_2 = 0$, $g_2 = 2.0$, $s_0 = 0.4$ and at $\varepsilon = 0.07$. Note that ε is well above the critical value $\varepsilon_c^{so} = 0.029$, and the sources are stable. Hence, any movement of the coherent structures is solely due to their interactions. Note that in the final stage of an annihilation event, the source moves most, while the sink stays almost put. Note also the similarity to Fig. 24 of [38]. (b) Hidden line plot of $|A_L|$ showing the annihilation process in detail.

Coullet et al. [48] briefly mention that below ε_c^{so}, sources are very sensitive to noise. We found that the average width of the breathing sources depends weakly on the strength of the noise, but have not investigated this issue in detail. The dependence on the noise should be clarified further.

Finally, after a long transient, the non-stationary sources below ε_c^{so} seem to be only very weakly time-dependent, and in some sense "near" a stationary source solution. Can this idea be made more precise?

- *Pinning and interactions.* Partly to explain the experimental observation of Alvarez et al. [33], we have conjectured that sources can be pinned to slight inhomogeneities, and that if they do, the selected wavenumber will vary with the local inhomogeneity. Moreover, stationary sources are then expected to exist below ε_c^{so} of the homogeneous system, in much the same way as boundary conditions can give rise to the existence of stable stationary sources below ε_c^{so} [52]. Again, a back-up of these conjectures is called for.

  As some of our simulations indicate (see Fig. 14), when sources and sinks get close to each other, they attract and eventually coalesce (or form a pair) in some characteristic fashion. Can this attraction be understood perturbatively?
- *Bimodal chaos.* One of our key observations is that the wavenumber selection induced by the sources allows for a bimodal instability for g_2 just above 1. For g_2 just below 1, similar behavior can be found [106]. The chaotic dynamics in these regimes involves the competition between the two modes in an essential way, and apart from [59,106], a detailed analysis of the dynamics here is lacking.
- *Subcritical bifurcations.* To what extent can our arguments be extended to the case of a weakly subcritical bifurcation? As we discussed in Section 6.2.2, this issue is of relevance to the experiments on binary mixtures.

  Finally, we stress that in most cases we have only shown examples of the possible types of behavior. A more systematic mapping out of the phase-space of the coupled CGL equations (2) and (3) may very well lead to additional surprises.

Acknowledgements

We would like to thank Guenter Ahlers, Tomas Bohr, Arnaud Chiffaudel, Pierre Coullet, Francois Daviaud, Lorenz Kramer, Natalie Mukolobwiez, Alan Newell, Willem van de Water, and Mingming Wu for interesting and enlightening discussions. In addition, we wish to thank Roberto Alvarez for a fruitful collaboration of which this work is an outgrowth. MvH acknowledges financial support from the Netherlands Organization for Scientific Research (NWO), and the EU under contract nr. ERBFMBICT 972554.

Appendix A. Coherent structures framework for the single CGL equation

A.1. The flow equations

In this appendix, we lay the groundwork for our analysis of the coupled equations by summarizing and simplifying the main ingredients of the analysis of [68,69] of the single CGL equation

$$\partial_t A = \varepsilon A + (1 + \mathrm{i}c_1)\partial_x^2 A - (1 - \mathrm{i}c_3)|A|^2 A. \tag{A.1}$$

Note that if a single mode is present, the coupled equations reduce to a single CGL written in the frame moving with the linear group velocity of this mode, *not* in the stationary frame.

As in Eq. (11), a coherent structure is defined as a solution whose time dependence amounts, apart from an overall time-dependent phase factor, to a uniform translation in time with velocity v:

$$A(x, t) := \mathrm{e}^{-\mathrm{i}\omega t}\hat{A}(x - vt) = \mathrm{e}^{-\mathrm{i}\omega t}\hat{A}(\xi). \tag{A.2}$$

Note that if the coherent structure approaches asymptotically a plane wave state for $\xi \to \infty$ or for $\xi \to -\infty$, the phase velocity of these waves would equal the propagation velocity of the coherent structures if ω would be 0. When $\omega \neq 0$, these two velocities differ.

For solutions of the form (A.2), $\partial_t = -\mathrm{i}\omega - v\partial_\xi$, so when we substitute the Ansatz (A.2) into the single CGL equation (A.1), we obtain the following ODE:

$$(-\mathrm{i}\omega - v\partial_\xi)\hat{A} = \varepsilon\hat{A} + (1 + \mathrm{i}c_1)\partial_\xi^2\hat{A} - (1 - \mathrm{i}c_3)|\hat{A}|^2\hat{A}. \tag{A.3}$$

Solutions of this ODE correspond to coherent structures of the CGL equation (A.1) and vice-versa [68,69].

To analyze the orbits of the ODE (A.3), it is useful to rewrite it as a set of coupled first order ODE's. To do so, it is convenient to write A in terms of its amplitude and phase

$$\hat{A}(\xi) := a(\xi)\mathrm{e}^{\mathrm{i}\phi(\xi)}, \tag{A.4}$$

where a and ϕ are real-valued. Substituting the representation (A.4) into the ODE (A.3) yields, after some trivial algebra

$$\partial_\xi a = \kappa a, \quad \partial_\xi \kappa = \mathcal{K}(a, q, \kappa), \quad \partial_\xi q = \mathcal{Q}(a, q, \kappa), \tag{A.5}$$

where q and κ are defined as

$$q := \partial_\xi \phi, \quad \kappa := (1/a)\partial_\xi a. \tag{A.6}$$

The fact that there is no fourth equation is due to the fact that the CGL equation is invariant under a uniform change of the phase of A, so that ϕ itself does not enter in the equations. The functions $\mathcal{K}$ and $\mathcal{Q}$ are given by [68,69]

$$\mathcal{K} := \frac{1}{1 + c_1^2}[c_1(-\omega - vq) - \varepsilon - v\kappa + (1 - c_1c_3)a^2] + q^2 - \kappa^2, \tag{A.7}$$

$$\mathcal{Q} := \frac{1}{1 + c_1^2}[(-\omega - vq) + c_1(v\kappa + \varepsilon) - (c_1 + c_3)a^2] - 2\kappa q. \tag{A.8}$$

At first sight it may appear somewhat puzzling that we write the equations in a form containing $\kappa = \partial_\xi \ln a$ instead of simply $\partial_\xi a$. One advantage is that it allows us to distinguish more clearly between various structures whose amplitudes vanish exponentially as $\xi \to \pm\infty$ – these are then still distinguished by different values of κ. Secondly,

the choice of κ in favor or $\partial_\xi a$ allow us to combine κ and q as the real and imaginary part of the logarithmic derivative of $\hat{A}$: we can rewrite (A.5) more compactly as

$$\partial_\xi z = -z^2 + \frac{1}{1+\mathrm{i}c_1}[-\varepsilon - \mathrm{i}\omega + (1-\mathrm{i}c_3)a^2 - vz]. \tag{A.9}$$

where $z := \partial_\xi \ln(\hat{A}) = \kappa + \mathrm{i}q$.

The fixed points of the ODE's have, according to (A.5), either $a = 0$ or $\kappa = 0$. The values of q and κ for the $a = 0$ fixed points are related through the dispersion relation of the linearized equation, or, what amounts to the same, by the equation obtained by setting the right-hand side of (A.9) equal to zero and taking $a = 0$. Following [68,69] we will refer to these fixed points as *linear fixed points*. We will denote them by $L_\pm$, where the index indicates the sign of κ. This means that the behavior near an L_+ fixed point corresponds to a situation in which the amplitude is growing away from zero to the right, while the behavior near an L_- fixed point describes the situation in which the amplitude a decays to zero.

Since a fixed point with $a \neq 0, \kappa = 0$ corresponds to nonlinear traveling waves, the corresponding fixed points are refered to as *nonlinear fixed points* [68,69]. We denote these by $N_\pm$, where the index now indicates the sign of the *nonlinear group velocity* s of the corresponding traveling wave [68,69]. Thus, since the index of N denotes the sign of the group velocity, the amplitude near an N_+ fixed point can either grow ($\kappa > 0$) or decay ($\kappa < 0$) with increasing ξ.

The coherent structures correspond to orbits which go from one of the fixed points to another one or back to the original one, and the counting analysis amounts to establishing the dimensions of the in-and outgoing manifolds of these fixed points. In combination with the number of free parameters (in this case v and ω), this yields the multiplicity of orbits connecting these fixed points, and therefore of the multiplicity of the corresponding coherent structures.

A.2. Fixed points and linear flow equations in their neighborhood

Since there are three flow equations (A.5), there are three eigenvalues of the linear flow near each fixed point. When we perform the counting analysis for these fixed points we will only need the signs of the real parts of the three eigenvalues, since these determine whether the flow along the corresponding eigendirection is inwards ($-$) or outwards ($+$). We will denote the signs by pluses and minuses, so that $L_-(+,+,-)$ denotes an L_- fixed point with two eigenvalues which have a positive real part, and one which has a negative real part.

From Eqs. (A.5) and (A.9), we obtain as fixed point equations

$$a\kappa = 0, \quad (1+\mathrm{i}c_1)z^2 + vz + \varepsilon + \mathrm{i}\omega - (1+\mathrm{i}c_3)a^2 = 0, \tag{A.10}$$

where $z := \kappa + iq$. From (A.10) we immediately obtain that fixed points either have $a = 0$ (linear fixed points denoted as L) or $a \neq 0, \kappa = 0$ (nonlinear fixed points denoted as N). Defining $\tilde{v} := v/(1+c_1^2)$ and $\tilde{a} := a/(1+c_1^2)$, the derivative of the flow (A.5) is given by the matrix:

$$\mathrm{DF} = \begin{pmatrix} \kappa & a & 0 \\ 2\tilde{a}(1-c_1c_3) & -2\kappa - \tilde{v} & 2q - c_1\tilde{v} \\ -2\tilde{a}(c_1+c_3) & -2q + c_1\tilde{v} & -2\kappa - \tilde{v} \end{pmatrix}. \tag{A.11}$$

Solving the fixed point equations (A.10) and calculating the eigenvalues of the matrix DF (A.11) yields the dimensions of the incoming and outgoing manifolds of these fixed points. Note that according to our convention, a fixed point with a two-dimensional outgoing and one-dimensional ingoing manifold is denoted as $(+,+,-)$.

We can restrict the calculations to the case of positive v, since the case of negative v can be found by the left–right symmetry operation: $\xi \to -\xi$, $v \to -v$, $z \to -z$.

A.3. The linear fixed points

For the linear fixed points $a = 0$, and from (A.10) we obtain as fixed-point equation:

$$(1 + \mathrm{i}c_1)z^2 + vz + \varepsilon + \mathrm{i}\omega = 0, \tag{A.12}$$

which has as solutions

$$z = \frac{-v \pm \sqrt{v^2 - 4(1 + \mathrm{i}c_1)(\varepsilon + \mathrm{i}\omega)}}{2(1 + \mathrm{i}c_1)}. \tag{A.13}$$

The linear fixed points come as a pair, and the left–right symmetry implies that for $v = 0$, the eigenvalues of these fixed points are opposite.

At these fixed points, the eigenvalues are given by

$$\kappa \text{ or } -\tilde{v} - 2\kappa \pm \mathrm{i}(c_1\tilde{v} - 2q). \tag{A.14}$$

To establish the signs of the real parts of the eigenvalues, we need to determine the signs of κ and $-\tilde{v} - 2\kappa$.

Let us first establish the signs of κ; this is important in establishing whether the evanescent wave decays to the left (L_+) or to the right (L_-). For $v = 0$, the Eq. (A.12) is purely quadratic, and so its solutions come in pairs $\pm(\kappa + iq)$. By expanding the square-root (A.14) for large v one obtains that in this case $\kappa = -v$ or $\kappa = -\varepsilon/v$; for large v, both κ's are negative. Solving Eq. (A.12) we find that κ changes sign when

$$q = \pm\sqrt{\varepsilon}, \quad v = \frac{c_1\varepsilon - \omega}{\sqrt{\varepsilon}}. \tag{A.15}$$

For $\varepsilon < 0$, these equations have no solutions, and in that case there always is a L_- and a L_+ fixed point. For $\varepsilon > 0$ and $v < (c_1\varepsilon - \omega)/\sqrt{\varepsilon}$ there also is a L_- and a L_+ fixed point; for large v, there are two L_- fixed points.

To determine the sign of $-\tilde{v} - 2\kappa$ note that from the solution (A.13), we obtain that $\kappa = -\tilde{v}/2 \pm \mathrm{Re}(\sqrt{\ldots}/\ldots)$. After some trivial rearranging this yields that $-\tilde{v} - 2\kappa$ has opposite sign for the pair of L fixed points; when one of them has two $+$'s, the other has two $-$'s.

In the case that we have a L_+ and a L_- fixed point the counting is as follows. For the L_+ fixed point, $-\tilde{v} - 2\kappa$ is negative since both v and κ are positive, and the eigenvalue structure is then $(+, -, -)$. The L_- fixed point then has one negative eigenvalue κ, and two positive eigenvalues coming from the $-\tilde{v} - 2\kappa$. For large v, both $\kappa's$ are negative, and we obtain a $L_-(+, +, -)$ and a $L_-(+, -, -)$ fixed point.

In summary, then, the counting for the linear fixed points is as follows:

$$\begin{aligned}
&\varepsilon < 0 \quad \text{all } v: && L_-(+,+,-)\, L_+(+,-,-),\\
&\varepsilon > 0 \quad \begin{cases} v < -v_{\mathrm{cL}}: & L_+(+,-,-)\, L_+(+,+,+),\\ |v| < v_{\mathrm{cL}}: & L_-(+,+,-)\, L_+(+,-,-),\\ v > v_{\mathrm{cL}}: & L_-(+,+,-)\, L_-(-,-,-), \end{cases}
\end{aligned} \tag{A.16}$$

where $v_{\mathrm{cL}} = |c_1\varepsilon - \omega|/\sqrt{\varepsilon}$.

A.4. The nonlinear fixed points

The analysis of the nonlinear fixed points goes along the same lines. Since the nonlinear fixed point has $\kappa = 0, z = \mathrm{i}q$, the fixed point equations become:

$$a^2 = \varepsilon - q^2, \quad q^2(c_1 + c_3) - vq - \omega - c_3\varepsilon = 0. \tag{A.17}$$

which yields

$$q = \frac{v \pm \sqrt{v^2 + 4(\omega + c_3\varepsilon)(c_1 + c_3)}}{2(c_1 + c_3)}. \tag{A.18}$$

So the nonlinear fixed points come as a pair.

To obtain the eigenvalues, we substitute $\kappa = 0$ in the (A.11) and obtain as a secular equation:

$$(1+c_1^2)\lambda^3 + 2v\lambda^2 + [2a^2(c_1c_3 - 1) + 4q^2(1 + c_1^2) - 4c_1qv + v^2]\lambda + [4a^2(c_1 + c_3)q - 2a^2v] = 0. \tag{A.19}$$

We only need to know the number of solution of the secular equation that have positive real part, and instead of solving the equation explicitly, we can proceed as follows.

For a we cubic equation of the form

$$p_3\lambda^3 + p_2\lambda^2 + p_1\lambda^1 + p_0, \tag{A.20}$$

where $p_3 > 0$, we may read off the signs of the real parts of the solution to this equation from the following table [68,69]:

$$\begin{aligned}
p_0 > 0 \left[\begin{array}{ll} p_2 > 0,\ p_1p_2 > p_0p_3: & (-,-,-)\ \text{(case i)}, \\ \text{else}: & (+,+,-)\ \text{(case ii)}, \end{array} \right. \\
p_0 < 0 \left[\begin{array}{ll} p_2 < 0,\ p_1p_2 < p_0p_3: & (+,+,+)\ \text{(case iii)}, \\ \text{else}: & (+,-,-)\ \text{(case iv)}. \end{array} \right.
\end{aligned} \tag{A.21}$$

According to these rules, there are three combinations of the coefficients that we need to now the sign of, being

$$p_0 = 4a^2q(c_1 + c_3) - 2a^2v, \tag{A.22}$$

$$p_2 = 2v, \tag{A.23}$$

$$p_1p_2 - p_0p_3 = -(1 + c_1^2)[4a^2(c_1 + c_3)q - 2a^2v] + 2v[2a^2(c_1c_3 - 1) + 4q^2(1 + c_1^2) - 4c_1qv + v^2]. \tag{A.24}$$

As before, we will take $v > 0$, which makes $p_2 > 0$.

The sign of p_0 is equal to the sign of $2q(c_1 + c_3) - v$, which according to Eq. (A.18) is either $\pm\sqrt{\ldots}$. The group velocity $\partial_q\omega$ of the the plane waves corresponding to the N fixed points is found from (A.17) to be $2q(c_1 + c_3) - v$, which can be rewritten as $p_0/(2a^2)$. So, we always have one N_- fixed point with $p_0 < 0$ and one N_+ fixed point with $p_0 > 0$.

When $p_0 < 0$, since p_2 is positive, the fixed point is $N_-(+,-,-)$ (case (iv)). When $p_0 > 0$, the eigenvalues depend on the sign of $p_1p_2 - p_0p_3$; when it is positive the eigenvalues are $(-,-,-)$, when it is negative, the eigenvalues are $(+,+,-)$. Defining v_{cN} as the value of $|v|$ where $p_1p_2 - p_0p_3$ changes sign, we obtain for the nonlinear fixed points:

$$\begin{array}{ll}
v < -v_{cN}: & N_-(+,+,+) \text{ and } N_+(+,+,-), \\
|v| < v_{cN}: & N_-(+,-,-) \text{ and } N_+(+,+,-), \\
v > v_{cN}: & N_-(+,-,-) \text{ and } N_+(-,-,-).
\end{array} \tag{A.25}$$

Eqs. (A.16) and (A.25) express the dimensions of the stable and unstable manifolds of the fixed points of the single CGL equation, and these are the basis for the counting arguments for coherent structures in this equation [68,69]. We now turn to the extension of these results to the coupled CGL equations.

Appendix B. Detailed counting for the coupled CGL equations

B.1. General considerations

While the counting for the coupled CGL equations follows unambiguously from that for the single CGL, there are various nontrivial subtleties in the extension of those results to the coupled CGL equations that require careful discussion.

Suppose we want to perform the counting for the $a_L = 0, \kappa_R = 0$ fixed point, which corresponds to the case in which only a right-traveling wave is present. The fixed point equations that follow from (15) are, up to a change of $v \to v - s_0$, equal to the fixed point equation for the nonlinear fixed points of the single CGL equation, and can be solved accordingly. To solve the fixed point equations that follow from (13), note that a_R is a constant at the fixed point and so the term $-g_2(1 - ic_2)a_R^2$ can be absorbed in the $-\varepsilon - i\omega_L$ term. Since we may choose ω_L freely, for the counting analysis we can forget about the $ig_2c_2a_R^2$ as we may think of it as having been absorbed into the frequency. The sign of $\varepsilon_{\text{eff}}^L$, defined in Eq. (18) to be $\varepsilon_{\text{eff}}^L = \varepsilon - g_2a_R^2$ will, however, be important. Likewise, at the other fixed point where $a_R = \kappa_L = 0$ the effective ε is $\varepsilon_{\text{eff}}^R = \varepsilon - g_2a_L^2$.

Since the fixed points we are interested in for sources and sinks always have either $a_L = 0$ or $a_R = 0$, the linearization around them largely parallels the analysis of the single CGL equation. For, when we linearize about the $a_L = 0$ fixed point, we do not have to take into account the variation of a_R in the coupling term and this allows us, for the counting argument, to absorb these terms into an effective ε and redefined ω as discussed above. Once this is done, the linear equations for the mode whose amplitude a vanishes at the fixed point *do not involve the other mode variables at all*. As a result, the matrix of coefficients of the linearized equations has a block structure, and most of the results follow directly from those of the single CGL equation. We will below demonstrate this explicitly, using a symbolic notation for various terms whose precise expression we do not need explicitly.

If we consider the 6 variables a_L, κ_L, q_L, a_R, κ_R and q_R as the elements of a vector w, and linearize the flow equations (A.5) about a fixed point where one of the modes is nonzero, we can write the linearized equations in the form $\dot{w}_i = \sum_j M_{ij}w_j$, where the 6×6 matrix M has the structure

$$M = \begin{pmatrix} \kappa_L & a_L & 0 & 0 & 0 & 0 \\ \text{“}a_L\text{”} & X & X & \text{“}a_R\text{”} & 0 & 0 \\ \text{“}a_L\text{”} & X & X & \text{“}a_R\text{”} & 0 & 0 \\ 0 & 0 & 0 & \kappa_R & a_R & 0 \\ \text{“}a_L\text{”} & 0 & 0 & \text{“}a_R\text{”} & X & X \\ \text{“}a_L\text{”} & 0 & 0 & \text{“}a_R\text{”} & X & X \end{pmatrix}. \tag{B.1}$$

In this expression, all quantities assume their fixed point values. Furthermore, “a_R” and “a_L” represent terms that are linear in a_R or a_L, and the X stand for longer expressions that we do not need at the moment. At the fixed points, either a_R or a_L is zero, so either the upper-right block is identical to zero, or the lower-left block is zero. *In either case, the eigenvalues are simply given by the eigenvalues of the upper-left and lower-right block-matrices*. This implies that for each of the 3×3 blocks, we can use the results of the counting for a single CGL equation, provided we take into account that v and ε should be replaced by $v \pm s_0$ and $\varepsilon_{\text{eff}}^L$ or $\varepsilon_{\text{eff}}^R$ at the appropriate places!

As discussed in Appendix A, the fixed point structure of the single CGL depends on two "critical" velocities, v_{cL} and v_{cN}, In general, these are different for the two fixed points which the orbit connects, so there is in principle a large number of possible regimes, each with their own combination of eigenvalue structures at the fixed points. An exhaustive list of all possibilities can be given, but it does not appear to be worthwhile to do so here. For, many of the exceptional cases occur for large values of the propagation velocity v and the relevance of the results for these solutions of the coupled CGL equations is questionable – after all, as we explained before, the counting can at most only demonstrate that certain solutions might be possible in some of these presumably somewhat extreme ranges of parameter values, but they by no means prove the existence of such solutions or their stability or dynamical relevance. Indeed, as discussed in Section 4.2, for small ε the sources are intrinsically dynamical and are not given by the *coherent* sources as obtained from the ODE's (12)–(15).

For these reasons, our discussion will be guided by the following observations. The sinks and sources observed in the heated wire experiments have velocities that are smaller that the group velocity [33] [16]; this also seems to hold for other typical experiments with finite linear group velocity s_0. This motivates us to start the discussion by investigating the regime that the velocity v is smaller than the linear group velocity, $|v| < s_0$. The sources are now as sketched in Fig. 1a and the sinks are as in Fig. 1c; this restriction already leads to a tremendous simplification. Furthermore, we are especially interested in the case that the two modes suppress each other sufficiently that the effective ε of the mode which is suppressed is negative, i.e., $\varepsilon_{\rm eff}^{\rm L/R} < 0$. This requirement is certainly fulfilled for sufficiently strong cross-coupling. The technical simplification of taking $\varepsilon_{\rm eff}^{\rm L/R} < 0$ is that in this case the structure of the linear fixed points is completely independent of the parameters v and ω – see Eq. (A.16). It should be noted, however, that in Section 5.2 we will encounter source/sink patterns where $\varepsilon_{\rm eff}$ is positive; these patterns are chaotic. Also, the *anomalous* sources and sinks, mentioned at the end of Section 3.1, can in some parameter ranges defy the general rules obtained here (see Section B.7 of this appendix). Furthermore, in Section B.6 we will discuss the cases $s_0 < 2q(c_1 + c_3)$ (i.e., sources and sinks corresponding to those of Fig. 1(b) and (d)), and the $s_0 = 0$ limit.

B.2. Multiplicities of sources and sinks

We will first perform the analysis starting with the restrictions given above. From Fig. 1 we can read off the building blocks of sources and sinks. are. We refer to the fixed point corresponding to $x \to -\infty(\infty)$ as fixed point 1(2). In the coupled CGL equation case, we refer to the total group velocity of the nonlinear waves, which is given by $2q(c_1 + c_3) + v \pm s_0$ [see Eqs. (9) and (10)]; since by the substitution $v \to v \pm s_0$ we absorb the s_0 in the v, the indexes of the N_- and N_+ fixed points correspond to the nonlinear group velocities in the co-moving frame of the coherent structures. For sinks of the type sketched in Fig. 1(c), $A_{\rm L} = 0$ for large negative x and $A_{\rm R} = 0$ for large positive x. Consequently, the flow is

$$\text{from } \begin{cases} N_+ & (v - s_0) \\ L_+ & (v + s_0) \end{cases} \text{ to } \begin{cases} L_- & (v - s_0) \\ N_- & (v + s_0) \end{cases} \tag{B.2}$$

For sources of the type sketched in Fig. 1(a), $A_{\rm R} = 0$ for large negative x and $A_{\rm L} = 0$ for large positive x. Consequently, the flow is

$$\text{from } \begin{cases} N_- & (v + s_0) \\ L_+ & (v - s_0) \end{cases} \text{ to } \begin{cases} L_- & (v + s_0) \\ N_+ & (v - s_0) \end{cases} . \tag{B.3}$$

[16] In the experiments of [33], it was estimated from the data that $s_0 \approx v_{\rm ph}/3$, where $v_{\rm ph}$ is the phase velocity, while typical sinks had a velocity v which could be as small as $v_{\rm ph}/50$.

As in Appendix A, we will denote the real parts of the three eigenvalues of the fixed points by a string of plus or minus signs; e.g. $(+,-,-)$.

For $\varepsilon_{\mathrm{eff}} < 0$ and arbitrary velocities, we obtain for the L fixed points (see Eqs. (A.16)):

$$L_-(+,+,-), \quad L_+(+,-,-). \tag{B.4}$$

For now we assume that $|v| < s_0$, $v - s_0 < 0$ and $v + s_0 > 0$. This yields, according to (A.25) for the N fixed points:

$$N_-(+,-,-), \quad N_+(+,+,-). \tag{B.5}$$

For sources we find that the combined (N_-, L_+) fixed point 1 has a two-dimensional outgoing manifold, which yields one free parameter. We can think of this parameter as a coordinate parameterizing the "directions" on the unstable manifold [17]. Now, the only other freedom we have for the trajectories out of fixed point 1 is associated with the freedom to view v, ω_{L} and ω_{R} as parameters in the flow equations that we can freely vary. This yields a total of four free parameters. Fixed point 2 (a (N_+, L_-) combination) has, according to Eqs. (B.3),(B.4) and (B.5), a four-dimensional outgoing manifold. An orbit starting from fixed point 1 has to be "perpendicular" to this manifold in order to flow to fixed point 2; this yields four conditions. Assuming that these conditions can be obeyed for some values of the free parameters, it is clear that as long as there are no accidental degeneracies, we expect that there is at most only a discrete set of solutions possible – in other words, solutions will be found for sets of isolated values of the angle, v, ω_{L} and ω_{R}. One refers to this as a discrete set of sources.

When we fix $v = 0$, there is the following symmetry that we have to take into account: $\xi \to -\xi$, $z_{\mathrm{L}} \leftrightarrow -z_{\mathrm{R}}$, $a_{\mathrm{L}} \leftrightarrow a_{\mathrm{R}}$. Furthermore, this left–right symmetry yields that we should take $\omega_{\mathrm{L}} = \omega_{\mathrm{R}}$, so, in comparison to the general case, we have two free parameters less. When the outgoing manifold of fixed point 1 intersects the hyper-plane $z_{\mathrm{L}} = -z_{\mathrm{R}}, a_{\mathrm{L}} = a_{\mathrm{R}}$, this yields, by symmetry, a heteroclinic orbit to fixed point 2. Therefore we only need to intersect the hyper-plane to obtain a heteroclinic orbit, which yields two conditions (instead of four in the general case). For the sources we have now two conditions and two free parameters; and this yields a discrete set of $v = 0$ sources. In other words, within the discrete set of sources we generically expect there to be a $v = 0$ source solution.

For a sink we obtain, combining (B.2),(B.4) and (B.5), that fixed point 1 (a (N_+, L_+) combination) has a three-dimensional outgoing manifold, which yields two free parameters, while fixed point 2 (a (N_-, L_-) combination) has a three-dimensional outgoing manifold, which yields three conditions to be satisfied. Together with the three free parameters v, ω_{L} and ω_{R}, this yields a two-parameter family of sinks.

B.3. The role of ε

When discussing the counting for the single CGL equation, the value of ε is uniquely determined. In the coupled equations however, one needs to work with the *effective* value of ε when studying the linear fixed points, since the growth of the linear modes are determined by renormalized values of ε which are given by $\varepsilon_{\mathrm{eff,L}} = \varepsilon - g_2 a_{\mathrm{R}}^2$, $\varepsilon_{\mathrm{eff,R}} = \varepsilon - g_2 a_{\mathrm{L}}^2$ for the left-and right-traveling modes respectively [see Eq. (18)]. While the inclusion of the sign structure of the linear fixed points for positive values of ε may have seemed somewhat superfluous for the *single* CGL equation, in the case of the coupled equations this is relevant. In the analysis in Sections B.4–B.6 we assume that both effective values of ε are negative. Some comments on the counting for positive values of $\varepsilon_{\mathrm{eff}}$ are given in Section B.7.

[17] Note that a one-dimensional manifold yields no free parameters other than the one associated with the trivial translation symmetry of the solution, and, in general, a p-dimensional outgoing manifold yields $p - 1$ nontrivial free parameters

B.4. The role of the coherent structure velocity v

In the counting for the single CGL equation, we were able to remove the group velocity term $\sim s_0$ by means of a Galilean transformation to the comoving frame. In the coupled equations this is not possible, however, and we need to incorporate the s_0-terms when studying the fixed point structure.

In particular, when translating the result for the single CGL into coupled CGL variables, we need to make the following replacements where v is concerned

$$\text{For the } a_{\mathrm{R}} \text{ mode}: v \to v - s_0 \equiv v_{\mathrm{R}}, \tag{B.6}$$

$$\text{For the } a_{\mathrm{L}} \text{ mode}: v \to v + s_0 \equiv v_{\mathrm{L}}. \tag{B.7}$$

Just like the possible occurrence of positive values of ε could possibly affect the linear fixed points, this may well affect the nonlinear fixed points. In the single CGL equation we were allowed to take $v \geq 0$, but we can no longer do this in the coupled case. Let us focus on the case $v = 0$, i.e, consider stationary coherent structures. Since s_0 is by definition positive, the a_{L} mode has $v_{\mathrm{L}} = s_0 > 0$, while the a_{R} has $v_{\mathrm{R}} = -s_0 < 0$. The statement that we can alway take $v > 0$ therefore no longer holds here, and we need to exercise caution when evaluating the nonlinear fixed points as well. In particular, *moving sources* ($v > 0$) with $|v_{\mathrm{R}}| > v_{\mathrm{cN}}$ or $v_{\mathrm{L}} > v_{\mathrm{cN}}$ can have different multiplicities than the stationary one with $v = 0$.

In the formulas for the counting, one should keep in mind that the linear group velocities have opposite signs for the left-and right moving modes: this is also apparent from Eqs. (9) and (10), where we defined $s_{0,\mathrm{R}} = s_0 = -s_{0,\mathrm{L}}$, so that we may write the nonlinear group velocities as

$$s_{\mathrm{R}} = s_{0,\mathrm{R}} + 2q_{\mathrm{R}}(c_1 + c_3), \quad s_{\mathrm{L}} = s_{0,\mathrm{L}} + 2q_{\mathrm{L}}(c_1 + c_3). \tag{B.8}$$

B.5. Normal sources always come in discrete sets

In this section, we show that it is not possible for normal stationary sources, i.e., sources whose s and s_0 have the same sign, and for whom $\varepsilon_{\mathrm{eff}} < 0$ for the linear modes, to come in families. The flow for a normal source is

$$\text{from } \begin{cases} A_{\mathrm{L}} : N_-(v + s_0) \\ A_{\mathrm{R}} : L_+(v - s_0) \end{cases} \text{ to } \begin{cases} A_{\mathrm{L}} : L_-(v + s_0) \\ A_{\mathrm{R}} : N_+(v - s_0) \end{cases}. \tag{B.9}$$

According to the counting, we have for the $N_-(v + s_0)$ fixed point on the left that (we take $v = 0$)

$$p_0 = 4a_{\mathrm{L}}^2 q_{\mathrm{L}}(c_1 + c_3) - 2a_{\mathrm{L}}^2 v_{\mathrm{L}} = 2a_{\mathrm{L}}^2[-s_0 + 2q_{\mathrm{L}}(c_1 + c_3)] = 2a_{\mathrm{L}}^2 s_{\mathrm{L}} < 0, \tag{B.10}$$

because for a normal source s_{L} has the same sign as $s_{0,\mathrm{L}}$. Furthermore we have

$$p_2 = 2v_{\mathrm{L}} = 2s_0 > 0. \tag{B.11}$$

This implies, according to Eq. (A.21), that the sign structure of the left fixed point is a $(N_-(+,-,-), L_+(+,-,-))$ combination, independent of the selected wavenumber of the nonlinear mode and the sign of the combination $p_1 p_2 - p_0 p_3$. The dimension of the outgoing manifold is therefore always equal to 2, yielding one free parameter. For the right fixed point, a completely similar argument yields an $(N_+(+,+,-), L_-(+,+,-))$ fixed point, again independent of the selected wavenumber or $\mathrm{sgn}[p_1 p_2 - p_0 p_3]$. We therefore have to satisfy four conditions at this fixed point.

Combining this with the free parameters we already had and the additional symmetry at $v = 0$ we find that the sources *always* come in discrete sets, independent of the selected wavenumbers and the parameters.

B.6. Counting for anomalous $v = 0$ sources

When the signs of the linear group velocity s_0 and the nonlinear group velocity s are opposite, we are dealing with anomalous sources. This section investigates the consequences this has for the counting of such sources.

For an anomalous source, cf. Fig. 1(b), the flow is (again we only consider $\varepsilon_{\mathrm{eff}} < 0$ for the linear modes)

$$\text{from } \begin{cases} A_{\mathrm{L}} : L_+(v + s_0) \\ A_{\mathrm{R}} : N_-(v - s_0) \end{cases} \text{ to } \begin{cases} A_{\mathrm{L}} : N_+(v + s_0) \\ A_{\mathrm{R}} : L_-(v - s_0) \end{cases}, \tag{B.12}$$

which yields for the nonlinear fixed point on the left

$$p_0 = 4a_{\mathrm{R}}^2 q_{\mathrm{R}}(c_1 + c_3) - 2a_{\mathrm{R}}^2 v_{\mathrm{R}} = 2a_{\mathrm{R}}^2[s_0 + 2q_{\mathrm{R}}(c_1 + c_3)] = 2a_{\mathrm{R}}^2 s_{\mathrm{R}} < 0. \tag{B.13}$$

where $\mathrm{sgn}[s_{\mathrm{R}}] = -\mathrm{sgn}[s_{0,\mathrm{R}}]$. Furthermore

$$p_2 = 2v_{\mathrm{R}} = -2s_0 < 0, \tag{B.14}$$

so that both p_0 and p_2 are negative, which implies that, according to Eq. (A.21), the sign structure of the N_- fixed point depends on $\mathrm{sgn}[p_1 p_2 - p_0 p_3]$. In particular, when $p_1 p_2 - p_0 p_3$ is negative it is $N_-(+,+,+)$, and if it is positive it is $N_-(+,-,-)$. If $p_1 p_2 - p_0 p_3 < 0$, we can perform a similar calculation for the right fixed point, and we find that the counting then yields a two-parameter family of anomalous sinks. If the expression is positive, however, we find that the anomalous sources also come in a discrete set.

The sign of this expression depends, for any given set of coefficients, on the selected wavenumber q_{sel} of the nonlinear mode, and therefore the wavenumber selection mechanism will determine whether we can actually get to a regime where sources come as a family. In practice, we have not found any examples where this happens. This suggests to us that the possible regions of parameters space where this might happen, are small.

B.7. Counting for anomalous structures with $\varepsilon_{\mathrm{eff}} > 0$ for the suppressed mode

As mentioned before, another situation that can change the counting is realized when the suppression of the effective ε by the nonlinear mode is not sufficiently large at the linear fixed points, so that $\varepsilon_{\mathrm{eff}} > 0$. If we restrict ourselves to the $v = 0$ case, Eq. (A.16) tell us that the counting may indeed change when in addition $|s_0| > v_{\mathrm{cL}}$. This implies that the multiplicity of sources and sinks changes dramatically under these circumstances. An insufficient suppression may happen in particular when g_2 is only slightly bigger than 1, while the selected wavenumber is large enough to lower the asymptotic value of the nonlinear amplitude significantly below its maximal value $\sqrt{\varepsilon}$. The zero mode then no longer stays suppressed; instead, it starts to grow, and we then typically get chaotic dynamics, see, e.g., Section 5.2. For this reason, we confine ourselves to a few brief observations concerning the $v = 0$ case.

For $v = 0$ and $\varepsilon_{\mathrm{eff}} > 0$, we can, according to Eq. (A.16), have a $L_-(---)$ fixed point of the A_{L} mode when $s_0 > v_{\mathrm{cL}}$. The A_{R} mode then has a $L_+(+,+,+)$ fixed point. Since the index of L denotes the sign of the asymptotic value of κ, with these fixed points we could in principle build a two-parameter family of stationary sources, provided s and s_0 have the same sign in the nonlinear region; otherwise the structures would be anomalous sinks.

Although we have not pursued the possible properties of such sources, we expect almost all members of this double family to be unstable. The reason for this is that when $\varepsilon_{\mathrm{eff}}$ is positive, the dynamics of the leading edge of the suppressed mode is essentially like that of a front propagating into an unstable state. As is well known [68,69], in that case there is also a two-parameter family of fronts in the CGL equation, but almost all of them are dynamically irrelevant.

Appendix C. Asymptotic behaviour of sinks for $\varepsilon \downarrow 0$

In this appendix, we will discuss the scaling of the width of sinks in the small-ε limit.

We will assume that in the domain to the left of the sink, the A_{R}-mode is suppressed, i.e., $\varepsilon_{\mathrm{eff}}^{\mathrm{L}} < 0$ (likewise to the right of the sink). As will be discussed in Section 5.2 below, we may get anomalous behavior when $\varepsilon_{\mathrm{eff,L}} > 0$, which can occur when $g_2 a_{\mathrm{R}}^2 < \varepsilon$; in that case the A_{L} mode is (weakly) unstable and various types of disordered behavior occur.

Assuming $\varepsilon_{\mathrm{eff}}^{\mathrm{L}}$ to be negative to the left of a sink, the amplitude of the left-traveling mode grows exponentially for increasing ξ as $|A_{\mathrm{L}}|(\xi) \sim \mathrm{e}^{\kappa_{\mathrm{L}}^{+}\xi}$. The spatial growth rate κ_{L} is given, by definition, by the value of κ at the linear fixed point. According to Eq. (A.13), one finds for $z_{\mathrm{L}} = \kappa_{\mathrm{L}} + \mathrm{i}q_{\mathrm{L}}$:

$$z_{\mathrm{L}} = \frac{-(v+s_0) \pm \sqrt{(v+s_0)^2 - 4(1+\mathrm{i}c_1)(\varepsilon_{\mathrm{eff,L}} + \mathrm{i}\omega)}}{2(1+\mathrm{i}c_1)}, \tag{C.1}$$

where we have used the fact that for the left-traveling mode, v as used in the appendix is replaced by $v + s_0$, and $\varepsilon_{\mathrm{eff,L}} = \varepsilon - g_2 a_{\mathrm{R}}^2$. If we expand the square-root in the small ε regime, where ω also tends to zero, we obtain

$$z_{\mathrm{L}} \approx \frac{-(v+s_0)}{2(1+\mathrm{i}c_1)} \pm \frac{(v+s_0)}{2(1+\mathrm{i}c_1)} \left[1 - \frac{2(1+\mathrm{i}c_1)(\varepsilon_{\mathrm{eff,L}} + \mathrm{i}\omega)}{(v+s_0)^2}\right]. \tag{C.2}$$

Since $\varepsilon_{\mathrm{eff,L}}$ is negative, and of order ε, the root z_{L}^{+} with the positive real part is therefore

$$z_{\mathrm{L}}^{+} \approx \frac{-\varepsilon_{\mathrm{eff,L}} - \mathrm{i}\omega}{(v+s_0)}, \tag{C.3}$$

so that κ_{L}^{+} scales with ε as

$$\kappa_{\mathrm{L}}^{+} = \mathrm{Re}[z_{\mathrm{L}}^{+}] \sim \varepsilon. \tag{C.4}$$

In order for the exponent in $|A_{\mathrm{L}}(\xi)| \sim \mathrm{e}^{\kappa_{+\mathrm{L}}\xi}$ to be of order unity, $\xi \sim \kappa_{\mathrm{L}}^{+-1} \sim \varepsilon^{-1}$, which shows that the width of the sinks will asymptotically scale as ε^{-1} for small ε.

References

[1] A.C. Newell, J.A. Whitehead, J. Fluid Mech. 38 (1969) 279.
[2] M.C. Cross, P.C. Hohenberg, Rev. Mod. Phys. 65 (1993) 851.
[3] A.C. Newell, T. Passot, J. Lega, Ann. Rev. Fluid Mech. 25 (1993) 399.
[4] For an elementary introduction to the amplitude equation approach, see, e.g., M. van Hecke, P.C. Hohenberg, W. van Saarloos, in: H. van Beijeren, M.H. Ernst (Eds.), Fundamental Problems in Statistical Mechanics VIII, North-Holland, Amsterdam, 1994.
[5] D. Walgraef, Spatio-temporal Pattern Formation, Springer, Berlin, 1996.
[6] P. Pelcé, Dynamics of Curved Fronts, Academic Publishers, New York, 1988.
[7] See, e.g., K. Kassner, Pattern Formation in Diffusion Limited Crystal Growth, World Scientific, Singapore, 1996.
[8] A.J. Simon, J. Bechhoefer, A. Libchaber, Phys. Rev. Lett. 61 (1988) 2574.
[9] See, e.g., M. Ginibre, A. Akamatsu, G. Faivre, Phys. Rev. E 56 (1997) 780 and references therein.
[10] E. Meron, Phys. Rep. 218 (1992) 1.
[11] Y. Couder, S. Michelland, M. Rabaud, H. Thomé, in: F.H. Busse, L. Kramer (Eds.), Nonlinear evolution of Spatio-Temporal Structures in Dissipative Continuous Systems, Plenum Press, New York, 1990.
[12] M. Rabaud, S. Michelland, Y. Couder, Phys. Rev. Lett. 64 (1990) 184.
[13] L. Pang, J.R. de Bruyn, Phys. Rev. Lett. 70 (1993) 1791.
[14] A. Buka, L. Kramer (Eds.), Pattern Formation in Liquid Crystals, Springer, New York, 1996.
[15] H. Flyvbjerg, J. Hertz, M.H. Jensen, O.G. Mouritsen, K. Sneppen (Eds.), Physics of Biological Systems, Springer, Heidelberg, 1997.
[16] For an example in the context of binary mixtures, see H. Riecke, Phys. Rev. Lett. 68 (1992) 301.

[17] For an example in the context of chemical waves, see M. Ipsen, Amplitude equations and normal forms, PhD Thesis, University of Copenhagen (unpublished)
[18] M. Ipsen, F. Hynne, P.G. Sørensen, Amplitude equation for reaction-diffusion systems with a Hopf bifurcation and a slow real mode, preprint, 1998.
[19] In the context of convection in liquid crystals, see M. Dennin, M. Treiber, L. Kramer, G. Ahlers, D.S. Cannell, Phys. Rev. Lett. 76 (1995) 319.
[20] In the context of Marangoni convection, see A.A. Golovin, A.A. Nepomnyashchy, L.M. Pismen, H. Riecke, Physica D 106 (1997) 131.
[21] D. Bensimon, A. Pumir, B.I. Shraiman, J. Physique France 50 (1989) 3089.
[22] W. Schöpf, W. Zimmerman, Phys. Rev. E 47 (1993) 1739.
[23] E.Y. Kuo, M.C. Cross, Phys. Rev. E 47 (1993) R2245.
[24] M. van Hecke, W. van Saarloos, Phys. Rev. E 55 (1997) R1259.
[25] J. Herrmann, F.H. Busse, J. Fluid Mech. 255 (1993) 183.
[26] M.C. Cross, Phys. Rev. A 38 (1988) 3593.
[27] M.C. Cross, Physica D 37 (1989) 315.
[28] E. Knobloch, J. de Luca, Nonlinearity 3 (1990) 975.
[29] E. Knobloch, Nonlocal amplitude equations, in: S. Kai (Ed.), Pattern Formation in Complex Dissipative Systems, World Scientific, 1992.
[30] C. Martel, J.M. Vega, Nonlinearity 9 (1996) 1129.
[31] J.M. Vega, SIAM J. Math. Anal. 24 (1993) 603.
[32] C. Martel, J.M. Vega, Nonlinearity 11 (1998) 105.
[33] R. Alvarez, M. van Hecke, W. van Saarloos, Phys. Rev. E 56 (1997) R1306.
[34] M. Dubois, F. Daviaud, O. Ronsin, P. Bergé, Physica D 61 (1992) 140.
[35] J.M. Vince, M. Dubois, Europhys. Lett. 20 (1992) 505.
[36] J.M. Vince, M. Dubois, Physica D 102 (1997) 93.
[37] P. Kolodner, D. Bensimon, C.M. Surko, Phys. Rev. Lett 60 (1988) 1723.
[38] P. Kolodner, Phys. Rev. A 46 (1992) 6452.
[39] P. Kolodner, Phys. Rev. E 50 (1994) 2731.
[40] N. Mukolobwiez, A. Chiffaudel, F. Daviaud, private communications.
[41] E. Kaplan, V. Steinberg, Phys. Rev. A 46 (1992) R2996.
[42] E. Kaplan, V. Steinberg, Phys. Rev. Lett. 71 (1993) 3291.
[43] J.-J. Perraud, A. De Wit, E. Dulos, P.D. Kepper, G. Dewel, P. Borckmans, Phys. Rev. Lett. 71 (1993) 1272.
[44] A. Joets, R. Ribotta, Phys. Rev. Lett. 60 (1988) 2164.
[45] A. Joets, R. Ribotta, Nonlinear Coherent Structures, Lecture Notes in Physics 353 (1990) 159.
[46] A. Joets, R. Ribotta, J. Stat. Phys. 64 (1991) 981.
[47] P. Coullet, C. Elphick, L. Gil, J. Lega, Phys. Rev. Lett. 59 (1987) 884.
[48] P. Coullet, T. Frisch, T. Plaza, Physica D 59 (1993) 75.
[49] B.A. Malomed, Phys. Rev. E 50 (1994) R3310.
[50] B.A. Malomed, A.A. Nepomnyaschy, M.I. Tribelsky, Phys. Rev. A 42 (1990) 7244.
[51] I. Aranson, L. Tsimring, Phys. Rev. Lett. 75 (1995) 3273.
[52] A.B. Rovinsky, A.M. Zhabotinsky, I.R. Epstein, Phys. Rev. E 56 (1997) 2412.
[53] M. Neufeld, D. Walgraef, M. San Miguel, Phys. Rev. E 54 (1996) 6344.
[54] J. Lega, J.M. Vince, J. Phys. 6 (1996) 1417.
[55] P. Manneville, Y. Pomeau, Philosophical Magazine A 48 (1983) 607.
[56] P. Coullet, S. Fauve, E. Tirapegui, J. Physique Lett. 46 (1985) L-787.
[57] H. Sakaguchi, Prog Theor Phys. 95 (1996) 823.
[58] H. Sakaguchi, Physica Scripta T67 (1996) 148.
[59] A. Amengual, E. Hernández-Garcia, R. Montagne, M. San Miguel, Phys. Rev. Lett. 78 (1997) 4379.
[60] L. Gil, Phys. Rev. Lett. 70 (1993) 162.
[61] M. San Miguel, Phys. Rev. Lett. 75 (1995) 425.
[62] H. Riecke, Europhys. Lett. 11 (1990) 213.
[63] B.I. Shraiman, A. Pumir, W. van Saarloos, P.C. Hohenberg, H. Chaté, M. Holen, Physica D 57 (1992) 241.
[64] H. Chaté, Nonlinearity 7 (1994) 185.
[65] D.A. Egolf, H.S. Greenside, Phys. Rev. Lett. 74 (1995) 1751.
[66] M. van Hecke, B.A. Malomed, Physica D 101 (1997) 131.
[67] M. van Hecke, Phys. Rev. Lett. 80 (1998) 1896.
[68] W. van Saarloos, P.C. Hohenberg, Physica D 56 (1992) 303.
[69] W. van Saarloos, P.C. Hohenberg, Physica D 69 (1993) 209.
[70] N. Bekki, K. Nozaki, Phys. Lett. A 110 (1985) 133.
[71] R. Conte, M. Musette, Physica D 69 (1993) 1.
[72] P. Marcq, H. Chaté, R. Conte, Physica D 73 (1994) 305.

[73] S. Popp, O. Stiller, I. Aranson, A. Weber, L. Kramer, Phys. Rev. Lett. 70 (1993) 3880.
[74] A. Doelman, Physica 97 (1996) 398.
[75] O. Thual, S. Fauve, J. Phys. France 49 (1988) 1829.
[76] S. Fauve, O. Thual, Phys. Rev. lett. 64 (1990) 282.
[77] V. Hakim, P. Jakobsen, O. Pomeau, Europhys. Lett. 11 (1990) 19.
[78] V. Hakim, P. Jakobsen, O. Pomeau, Eur. J. Mech. B 10 (1991) 137.
[79] C. Elphick, E. Meron, Phys. Rev. A 40 (1989) 3226;.
[80] C. Elphick, E. Meron, Phys. Rev. Lett. 65 (1990) 2476.
[81] L. Kramer, E. Ben-Jacob, H. Brand, Phys. Rev. Lett. 49 (1982) 1891.
[82] G. Dee, J.S. Langer, Phys. Rev. Lett. 50 (1983) 383.
[83] E. Ben-Jacob, H. Brand, G. Dee, L. Kramer, J.S. Langer, Physica D 14 (1985) 348.
[84] W. van Saarloos, Phys. Rev. A 37 (1988) 211.
[85] W. van Saarloos, Phys. Rev. A 39 (1989) 6367.
[86] A.N. Stokes, Math. Biosci. 31 (1976) 307.
[87] G.C. Paquette, L.-Y. Chen, N. Goldenfeld, Y. Oono, Phys. Rev. Lett. 72 (1994) 76.
[88] U. Ebert, W. van Saarloos, Phys. Rev. Lett. 80 (1998) 1650.
[89] U. Ebert, W. van Saarloos, Fronts propagating uniformly into unstable states: Universal algebraic rate of convergence of pulled fronts, Physica D, in press.
[90] T. Kapitula, B. Sandstede, Physica D 124 (1998) 58–103.
[91] T. Kapitula, B. Sandstede, J. Opt. Soc. of America B15 (1998) 2757-2762
[92] J. Yang, D.J. Kaup, Solitary waves in perturbed generalized nonlinear Schroedinger equations, preprint, Dec. 1997.
[93] M. van Hecke, E. de Wit, W. van Saarloos, Phys. Rev. Lett. 75 (1995) 3830.
[94] R.J. Deissler, H.R. Brand, Phys. Rev. Lett. 72 (1994) 478.
[95] R.J. Deissler, H.R. Brand, Phys. Rev. Lett. 74 (1995) 4847.
[96] E. de Wit, Masters Thesis, unpublished.
[97] A. Couairon, J.-M. Chomaz, Primary and secondary nonlinear global instability, preprint, 1999.
[98] D. Bensimon, B.I. Shraiman, V. Croquette, Phys. Rev. A 38 (1988) 5461.
[99] P. Huerre, P.A. Monkewitz, Annu. Rev. Fluid Mech. 22 (1990) 473.
[100] A. Couairon, J.-M. Chomaz, Physica D 108 (1997) 236.
[101] P. Hagan, SIAM J. Appl. Math. 42 (1982) 762.
[102] A. Weber, L. Kramer, I.S. Aranson, L. Aranson, Physica D 61 (1992) 279.
[103] T. Bohr, G. Huber, E. Ott, Physica D 106 (1997) 95.
[104] I.S. Aranson, L. Aranson, L. Kramer, A. Weber, Phys. Rev. A 46 (1992) 2992.
[105] T. Bohr, M.H. Jensen, G. Paladin, A. Vulpiani, Dynamical Systems Approach to Turbulence, Cambridge, 1998, in press.
[106] H. Riecke, L. Kramer, The stability of standing waves, patt-sol/9805005, 1998.
[107] S. Ciliberto, P. Bigazzi, Phys. Rev. Lett. 60 (1988) 286.
[108] F. Daviaud, J. Lega, P. Bergé, P. Coullet, M. Dubois, Physica D 55 (1992) 287.
[109] E. Moses, J. Fineberg, V. Steinberg, Phys. Rev. A. 35 (1987) 2757.
[110] A.G.W. Baxter, K.D. Eaton, C.M. Surko, Phys. Rev. A 46 (1992) 1735.
[111] E. Kaplan, V. Steinberg, Phys. Rev. E 48 (1993) R641.
[112] See sections V.B.c.(iii) and X.A.6.a of [2], and references therein.
[113] A. Garcimartín, N. Mukolobwiez, F. Daviaud, Phys. Rev. E 56 (1997) 1699.
[114] N. Mukolobwiez, Thesis, Université Paris XI, 1998, unpublished.
[115] N. Mukolobwiez, A. Chiffuadel, F. Daviaud, Phys. Rev. Lett. 80 (1998) 4661.
[116] H. Herrero, H. Riecke, Physica D 85 (1995) 79, see also chao-dyn 9701017.
[117] H. Riecke, W.-J. Rappel, Phys. Rev. Lett. 76 (1996) 4035.